Design and Analysis of Modular Mechanisms for Flexible Reconfiguration in Robotics

A. Morales Gallegos[1], R. Torres-Córdoba[1], E. Magid[2], E. A. Martínez-García[1] *

[1]*Institute of Engineering and Technology*
Universidad Autónoma de Ciudad Juárez, Mexico

[3]*Institute of Information Technology and Intelligent Systems*
Kazan Federal University, Russian Federation

Abstract

Flexible reconfiguration in robotics pertains to a robotic system's capacity to dynamically adjust its configuration to meet diverse tasks, environmental demands, or operational specifications. This involves the deliberate design of robots with the capability to modify their physical structures, including joint arrangements, links, or components, to efficiently execute a spectrum of tasks. This study introduces the analysis and design of a modular mechanism aimed at morphological reconfiguration in robotic platforms. This adaptability enhances the versatility of robots, enabling them to adeptly handle a variety of tasks in diverse scenarios. The proposed mechanisms and technologies encompass modular designs, adjustable joints, and the capability to seamlessly switch between different end-effectors. The system comprises three gear systems and a joint featuring a convex-toothed sphere. These gears facilitate rotation along pitch and yaw axes, while an internal gear system, utilizing a planetary mechanism, propels a prismatic piston via a screw mechanism. The mathematical modeling, employing Lagrangian mechanics, illustrates globalized dynamics. Control models, grounded in a spherical coordinate model, are scrutinized by deducing the Jacobian matrix. Demonstrating diverse robotic platform configurations, this work exemplifies the concept of flexible reconfiguration, wherein robots adeptly manage varied and dynamic tasks without necessitating manual adjustments or reprogramming. Emphasizing the modeling and numerical simulations of motion analysis, this paper delves into the design of a joint mechanism contributing to the dynamic adaptability and reconfigurability of robots across various tasks.

Keywords: *reconfigurability, robot modeling, mechanism dynamics, model-based control*

1 Introduction

Robotic platforms are extensively utilized across various industries, ranging from manufacturing and entertainment to home services, transportation, construction, education, scientific research, surveillance, security, manufacturing, and search and rescue operations. Over time, the adoption

*Edgar A. Martínez-García. (edmartin@uacj.mx)
Alejandra Morales Gallegos (al173527@alumnos.uacj.mx)
Rafael Torres-Córdoba (ratorres@uacj.mx)
Evgeni Magid (magid@it.kfu.ru)

of robotic applications has experienced exponential growth. However, the efficacy of these platforms hinges on their ability to adapt to the specific tasks required in a given environment. For instance, robotic arms are meticulously designed for tasks such as assembly, selection, inspection, manufacturing, and material manipulation. These tasks necessitate platform models with varying morphological designs, tailored to the specific workspace and application requirements. Traditional robotic platforms, with fixed morphologies, may excel in performing specific tasks but could be poorly suited for a broader range of applications within the same environment.

On the contrary, directing research and development efforts towards physically reconfigurable robotic platforms can yield significant advantages. These platforms boast the capability to morph or adjust their physical structures to suit a broader range of tasks within a single environment. Such flexibility empowers them to capitalize on commercial opportunities more efficiently, as they can be customized to fulfill diverse tasks without requiring distinct specialized platforms. As a result, physically reconfigurable robotic platforms emerge as a more versatile solution for tackling a spectrum of tasks across different environments, ultimately enhancing their commercial viability and practicality. To enable a robot to change functionality with good performance in its programmed mission, the reconfiguration function must be practical and/or semi-automatic in the new task. Robotic reconfiguration, as a new physical capability, provides significant benefits in many daily activities of society. The applications of reconfigurable robots need to be sophisticated through engineering techniques to make them incredibly diverse. Advances in robotic engineering tend towards the modularization, reconfiguration, and self-reconfiguration of robots[3], allowing the extension of different physical and functional parts of the robot [1]. Robotics has permeated numerous sectors, with industry standing prominently among them. In industrial landscapes, the incorporation of modularized robotic platforms offers a myriad of advantages, from cost-saving measures to space optimization. By employing fewer robotic platforms, daily tasks can be executed more efficiently. Yet, the implications of robotic reconfiguration extend far beyond industrial confines. The integration of reconfigurable robots holds the promise of transformative changes in both individual lives and societal paradigms.

This research is dedicated to crafting and modeling a highly adaptable module poised to configure and reconfigure robotic platforms with a spectrum of morphologies and functionalities. It highlights different assembly morphologies for robotic platforms, offering an array of potential reconfigurations spanning walking, rolling, and robotic arms. The primary objective is to seamlessly integrate modularity within robotic platforms, streamlining reconfiguration processes and synchronized control to amplify their capabilities. This entails a meticulous design and modeling approach, culminating in a modular mechanism capable of dynamically reshaping complex robotic structures when interconnected and replicated. Such a mechanism is imbued with synchronization functions and locomotion control algorithms to ensure suitable performance across diverse configurations. Moreover, the study embarks on designing a mechanized system featuring both rotary and prismatic articulations, augmented with redundant sensory capabilities for precise and responsive actuation. This involves an exhaustive exploration of motion dynamics and control algorithms, complemented by the development of observability models tailored to the modular robotic architecture. Additionally, the research entails formulating controller schemes tailored to accommodate the intricacies of diverse robotic reconfigurations, further enriching the platform's adaptability and versatility. Through the development of a modularized robotic mechanism and its mechanical pluralization, a realm of robotic reconfiguration unfolds, broadening the spectrum of tasks achievable by a robotic platform.

In Section 2, we review research akin to our project, delving into recent works on related themes and delineating a robust conceptual framework. Transitioning to Section 3, we showcase the CAD software design of the modular mechanism, while Section 4 offers comprehensive insights into its instrumentation. Section 5 outlines the modeling of motion geometry for the module

mechanisms, alongside dynamic and kinematic models. Chapter 6 introduces the local position and velocity models, along with sophisticated global control models. Simultaneously, Section 7 explores diverse sample configurations and their functional reconfiguration. In Section 8 discusses some analysis about the results. Finally, section 9 encapsulates the conclusions derived from this comprehensive study.

2 Related Work

This section discusses some essential concepts and offers a comprehensive review of contemporary literature that supports the ongoing endeavor. Investigation into the reconfiguration and modularization of robotic structures encompasses a broad range of intricate subjects that have been consistently pursued over the years. Modularization, as a fundamental principle, streamlines construction optimization by integrating functional components designed for diverse elements.

Research efforts aimed at engineering precisely tailored models to improve stability, particularly in navigating challenging and uneven terrains encountered by quadruped robots, have been extensively explored. In the study conducted by Kula et al. [4], a comprehensive investigation delves into the realm of reconfigurable limbs for walking robots. The research examines the mechanical synthesis required to redefine walking cycloids, resulting in insights and showcasing the ability to optimize walking trajectories. This optimization renders the robots highly adaptable to diverse terrains, thereby significantly enhancing their overall performance. Techniques aimed at achieving robotic modularization and reconfiguration to enhance navigation across diverse multi-obstacle environments and terrains are pertinent in the field of reconfigurable robotics. The work [6] introduced the design and motion planning of a metamorphic reconfiguration walking robot and categorize walking robots into distinct types based on their structure, each offering unique movement characteristics. Furthermore, robotic reconfiguration emphasizes adaptable configurations to optimize performance tailored to specific tasks, such as adjusting the degrees of freedom within a structure. As demonstrated by the work [1], the proposed robot was reconfigured for machining tasks with varying numbers of axes, achieved through module reassembly and joint locking. In another context, modular configurability, which allows for multiple degrees of freedom in movement, represents specific instances of functional self-reconfigurability. The work [2] focused on the design and locomotive control of a morphologically variable parallel sub-actuated wing, emphasizing the need for optimal performance across different flight phases. Nevertheless, robots constructed using origami approaches leverage folding and unfolding mechanisms for self-assembly and movement. This results in lightweight, cost-effective solutions that are adaptable to diverse applications. For instance, the work reported by [8] proposed the creation of a reconfigurable robot utilizing origami techniques, which showed significant advantages including compact size, reduced manufacturing complexity, and the utilization of easily foldable materials. Previous research has yielded modular self-assembling robotic structures. For instance, inspired by social insects like ants and swarm robotics involved simple robotic structures interconnecting to form complex structures [9]. Furthermore, mudular self-assembling approaches [10], and refined for compactness [11]. The study by [12] presented a self-assembling and self-repairing robotic structure, demonstrating concurrent self-repair and assembly during assigned tasks. Furthermore, the principles of modularization and reconfiguration in robotics are also applied to agricultural tasks, where robotic machinery is utilized for a multitude of purposes. The work by [13] presented a conceptual modularized robotic platform capable of monitoring, harvesting, and fumigation in agriculture. To tackle the challenge of rewiring during modular addition and removal, the study by [14] introduced a reconfigurable modular humanoid architecture. This architecture incorporated actuators specifically engineered for mechanical and electrical compatibility between modules. Real-time communication interfaces between modules facilitating autonomous collec-

tive integration. Environmental interaction considerations are key application domains for robotic modularization and reconfiguration. The work [15] designed a modular robotic platform for life support applications, emphasizing flexible indoor movement within confined spaces. Similarly, [16] optimized the movement of a reconfigurable robot for pavement and sidewalk cleaning, with a turning mechanism for maneuverability in confined spaces while avoiding collisions. The challenge of terrain-dependent movement for reconfigurable robots is addressed by [17], utilizing semantic segmentation for object perception. Besides, the study by [18] introduced a reconfigurable quadruped/biped robot for aiding the elderly and disabled, capable of adjusting its walking form for stability and user safety based on the terrain. The topology of a reconfigurable modular robot significantly influences its performance. The study [19] determined optimal geometry to enhance performance, while the work [20] suggested a modeling method for kinematic analysis based on module coordinate systems, facilitating comprehensive characterization of module interactions.

The distinctive analysis of related work in Table 1 summarizes how our study findings compare with existing research.

Table 1: Comparison of key aspects between this study and related research.

Key features	**Related work**	**This study distinctions**
Motion geometry optimization for enhancing performance.	[4] [16][19]	Dynamic-based motion control of modules multi-function robots.
Metamorphic walking, adaptive locomotion and reconfigurable adaptable modules.	[6][14] [18]	Adaptable modules to craft structures.
Adjusting structural DOFs.	[1]	Module's functions reconfiguration.
Modular wing configurability.	[2]	Crafting adaptable modules.
Reconfigurable origami robotics.	[8]	Assembling adaptable modules.
Self-assembling/repairing structure.	[12]	Enabling module's functions.
Agriculture modular robotics.	[13]	Multi-function adaptable modules.
Modular robot for flexible capabilities.	[15]	To craft adaptable modules for morphological configurations.
Robot reconfiguration for diverse terrain-dependant navigation.	[17] [3]	Crafting modules for multiple robotic tasks.
Kinematic analysis for modular robotics.	[20]	Euler-Lagrange analysis.

Despite substantial progress in robotic reconfiguration, the vast scope of potential applications for modularization and reconfiguration necessitates continued exploration and refinement. This work specifically focuses on enhancing the mechanical design of the actuator responsible for providing movement to the robotic platform, aiming to expand degrees of freedom and achieve a broader range of motion.

3 Modular mechanism design

In this section, the proposed physical system design of the modular mechanism is presented, depicted in a CAD model. The proposed module mechanism includes three gear systems that, together, provide both rotational and prismatic movement. These gear systems offer 6 degrees of freedom (DOF) concerning the workspace, and in conjunction with its exterior design, allow for modularity. This work utilizes the rotation mechanisms yaw and pitch as illustrated in Figure

1, along with the spherical joint shown in Figure 2, and the prismatic movement mechanism in Figure 3. The central issue of this joint mechanisms consists of a toothed sphere or ball joint, with the orthogonal crossing of connected elements to control the degrees of freedom using a spherical coordinate approach.

3.1 Rotary motion mechanisms

The rotational movements of the module, according to the inertial system in Figure 2, are provided by the pitch mechanism (Figure 1b) and the yaw mechanism (Figure 1a), which offer rotation in pitch, yaw, and combined movements that also include roll.

According to the yaw mechanism shown in Figure 1a, we have, in the first place, the straight gear e_{20} transmitting the driving motion. This motion reaches the worm gear, consisting of g_{21} and e_{22}, which serves the same purpose as in the case of the pitch system: to increase power and stabilize the load applied to the module. The cylindrical gear e_{24} essentially functions as the final transmitter of the yaw rotation.

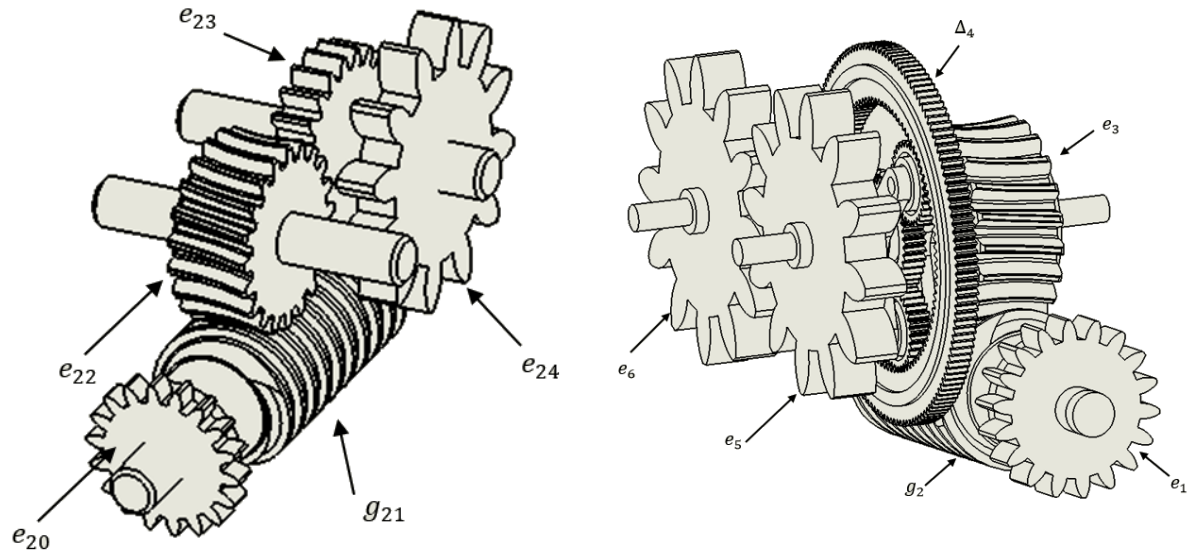

(a) *Yaw mechanism.* (b) *Pitch mechanism.*

Figure 1: Mecanismos yaw y pitch

In addition, the pitch mechanism (Figure 1b) tha ussually deals against gravity forces, initiates the driving motion at the straight gear e_1, which is powered by an electric motor. Subsequently, the motion is transmitted to the worm gear, commonly referred to as a worm, consisting of g_2 and e_3, which increases power and stabilizes the load posture. The helical gear e_3 has, on one side, a system of cylindrical planetary gears Δ_4 with a sun, three planets, and a straight ring gear, and on the other side, a pair of output cylindrical gears e_5 and e_6. The planetary system called Δ_4 provides high torque to the system. Gears e_5 and e_6 also provide additional torque and function as the final transmitters of the pitch rotation. Further analytical discussion of this notation is provided in more detail later in Definition 1.

Furthermore, the pitch and yaw mechanisms serve to transfer their respective movements to the spherical joint, as depicted in Figure 2, thereby effectuating the output motion of the module. To ensure the proper transmission of movement, both the toothed sphere and the final gears of the yaw and pitch mechanisms were designed with identical modules. This design consideration facilitates seamless movement transfer.

As a consequence of the resulting torque and power generated within the pitch and yaw mechanisms, there is an amplification of torque at the spherical joint. This increased torque is essential for enabling the module to support the interconnection of other modules and accessories effectively.

Figure 2 illustrates the arrangement of the gear systems in conjunction with the spherical joint, providing a visual representation of their integration.

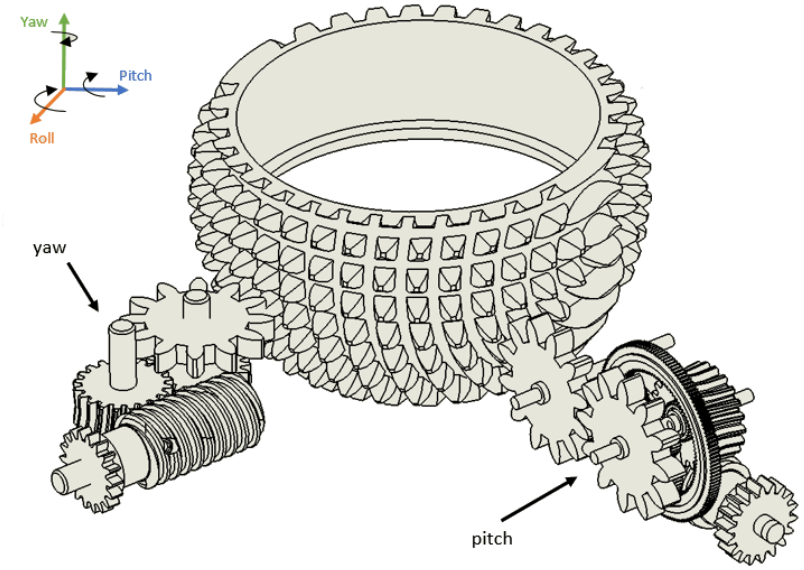

Figure 2: *Semi-spherical joint connected to the yaw and pitch mechanisms.*

3.2 Prismatic motion mechanism

The spherical joint, integral to the system's functionality, is manipulated via angular coordinates applied to its peripheral surface. Its design incorporates a hollow structure to house a third gear system, as illustrated in Figure 3b. This thoughtful arrangement serves to streamline the transmission of motion to a linked component featuring a screw mechanism. This screw mechanism, depicted in Figure 3a, enables the module's prismatic movement, allowing for controlled linear motion along a defined axis. This integration of components not only enhances the versatility of the module but also ensures precise and efficient movement, contributing to the overall effectiveness of the system.

The gear system in question is characterized by its intricate planetary configuration, which consists of two distinct subsystems operating in parallel. At the core of the primary system lies the sun gear denoted as e_{s30}, serving as the primary driving cylindrical gear. Working in tandem with this sun gear are four cylindrical planets, labeled as e_{p31}, e_{p32}, e_{p33}, and e_{p34}.

Adjacent to this primary system lies a secondary planetary arrangement, featuring its own sun gear, e_{s35}, and an additional set of four planets: e_{p36}, e_{p37}, e_{p38}, and e_{p39}. The intricate interplay of these gears and planets is depicted in Figure 4a.

Encompassing both planetary systems is a single crown gear, captured in the illustration presented in Figure 4b. This crown gear acts as a pivotal component in the overall mechanism, facilitating smooth and efficient motion transmission between the various gears.

The stacking of these planetary systems one atop the other, as showcased in Figure 4c, serves a dual purpose. Not only does it enable a substantial reduction in rotational speed, but it also significantly amplifies the torque output within a confined spatial footprint.

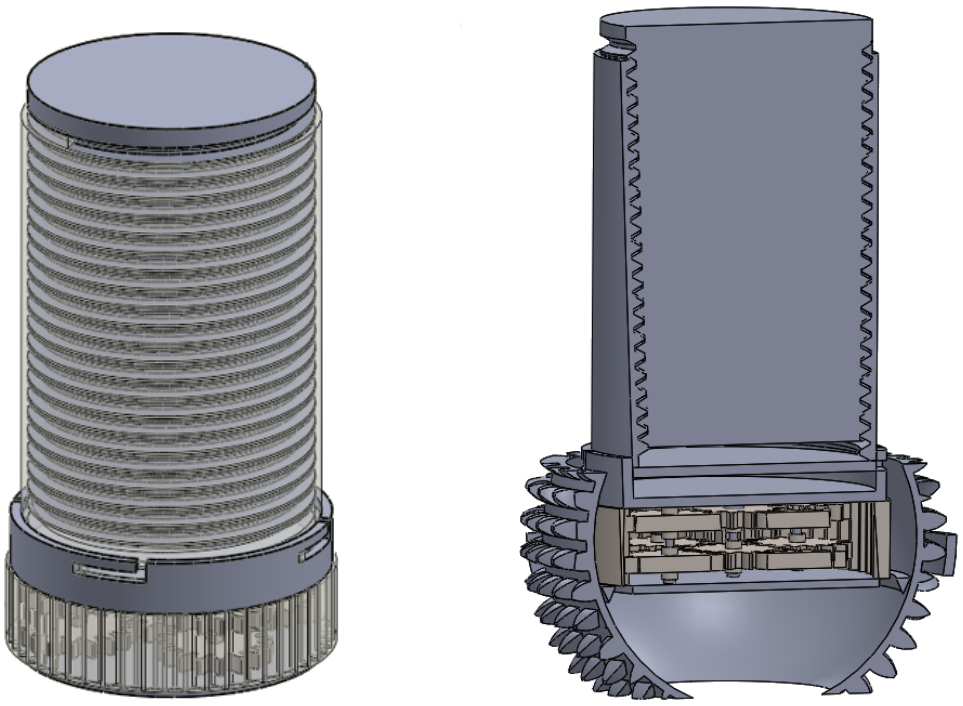

(a) *Screw piston prismatic link.* (b) *Primatic screw piston section view.*

Figure 3: Different views of the prismatic mechanism.

This thoughtful configuration underscores the attention to detail in the design process, aimed at improving both power transmission efficiency and space utilization. By integrating these planetary systems, the mechanism achieves improved performance and functionality, making it an indispensable component in the larger modular system.

Encircling the intricate arrangement of planetary gears lies the crown gear, serving as the pivotal component in transmitting motion to the prismatic axis of the screw-type piston. When the prismatic mechanism is set into motion, the rotational movement of the crown gear initiates the extension of the axis.

As the crown gear rotates, its engagement with the planetary gears facilitates the smooth transmission of motion along the prismatic axis. This dynamics ensures precise and controlled extension of the axis, enabling the module to execute its intended function effectively.

The coordinated movement between the crown gear and the planetary gears illustrates the proposed engineering behind the mechanism's design. By integrating these components, the system achieves motion transmission, contributing to its overall reliability and performance.

Figure 5b provides a comprehensive visual depiction showcasing both the interior and exterior views of the module. The interior image offers a detailed glimpse into the intricate mechanisms and components nestled within the module's structure, highlighting the complexity of its design and functionality. Meanwhile, the exterior view offers a broader perspective, revealing the module's overall form and configuration in its entirety.

Through these images, the readers gain valuable insights into the module's inner workings and external appearance, further showing its capabilities and potential applications. This comprehensive representation serves to enhance understanding and appreciation of the module's design and construction, underscoring its significance within the broader context of modular robotics approach of this study.

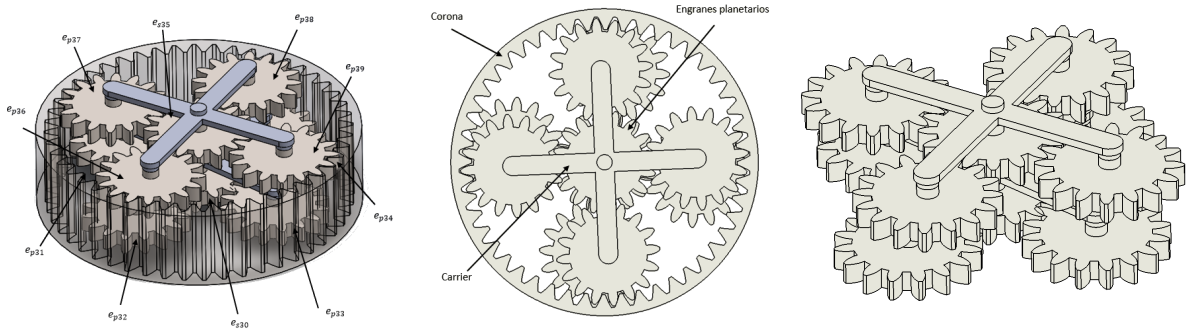

(a) *Perpespective view.* (b) *top view.* (c) *Dual planetary gearing.*

Figure 4: Prismatic mechanism based on a dual cascade planetary gearing system.

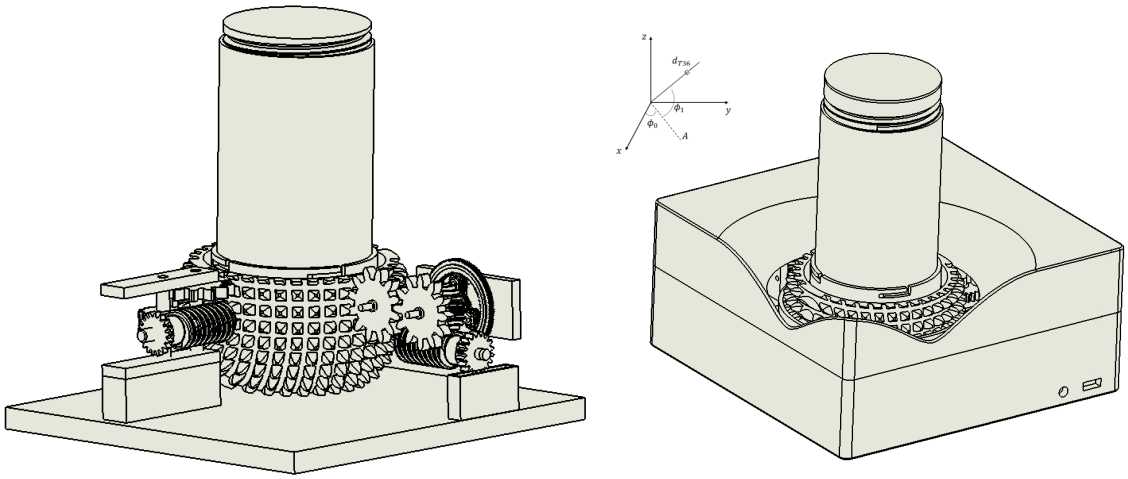

(a) *Joint's inner mechanisms.* (b) *External appearance.*

Figure 5: Inner and external joint's views.

4 Module instrumentation

Each mechanism, including pitch, yaw, and prismatic motion, is driven by its dedicated motor, ensuring asynchronous actuation. These motors serve as the driving force behind the module's various movements, providing the propulsion for each mechanism's function. To exert fine control over the speed of these motors, the Pulse Width Modulation (PWM) method is employed.

Through PWM, the system achieves unparalleled control over the motors' rotational speed by adjusting the width of the electrical pulses supplied to them. This approach allows for seamless modulation of motor speed, enabling smooth and accurate adjustments tailored to the specific requirements of each task. By leveraging PWM for speed control, the modular system attains enhanced efficiency and responsiveness across all mechanisms. This approach to motor control not only improves performance but also ensures robust execution of tasks in diverse environments, underlining the system's versatility and reliability.

Within each of the pitch, yaw, and prismatic gear systems, specialized motors are employed, each equipped with an encoder boasting a high resolution pulses per revolution. This high-resolution encoder plays a pivotal role in the system, enabling precise measurements crucial for accurately determining both position and velocity. The angular position model, derived from these measurements, serves as a cornerstone in the system's physical sensing. This model provides insights into the exact orientation and movement of the mechanisms, forming the basis for informed

decision-making and control strategies. Through the integration of these high-resolution encoders and analytical position models, the system attains accuracy and reliability in its motion control capabilities. This issue ensures operation and precise execution of tasks across diverse scenarios, for suitable performance and functionality.

The model for sensing the motor's angle is articulated in terms of a digital pulse train, as depicted by Equation (1):

$$\phi(\eta) = \frac{2\pi}{R}\eta_t \tag{1}$$

In this context, ϕ symbolizes the position angle in radians, η_t represents the instantaneous digital pulses (dimensionless), and R denotes the angular resolution coefficient measured in pulses per revolution. This model allows us to precisely determine the angle of the motor based on the pulse count received.

Furthermore, leveraging this angular model and its derivative, we can calculate the angular velocity. To initiate this process, we employ the Taylor series:

$$\phi_2 \approx \frac{\phi}{0!}(t_2 - t_1)^0 + \frac{\dot{\phi}}{1!}(t_2 - t_1)^1 + \frac{\ddot{\phi}}{2!}(t_2 - t_1)^2 + ... \tag{2}$$

By truncating at the second term or first derivative, the following expression captures the effect of two pulse readings at times t_1 and t_2.

$$\dot{\phi}(t, \eta) = \frac{\phi(\eta_2) - \phi(\eta_1)}{t_2 - t_1}, \tag{3}$$

Substituting (1) into (3), we obtain:

$$\dot{\phi}(\eta) = \frac{\frac{2\pi}{R}\eta_2 - \frac{2\pi}{R}\eta_1}{t_2 - t_1}, \tag{4}$$

upon factoring, we obtain:

$$\dot{\phi}(\eta) = \frac{2\pi}{R}\left(\frac{\eta_2 - \eta_1}{t_2 - t_1}\right) = \frac{2\pi}{R}\left(\frac{\Delta\eta}{\Delta t}\right). \tag{5}$$

Furthermore, the model for linear displacement, which plays a crucial role in our analysis,

$$s(\eta) = \frac{2\pi r}{R}\eta. \tag{6}$$

Hence, by differentiating to determine linear velocity using the Taylor series, (2):

$$\frac{ds}{dt}(\eta) = v(\eta) = \frac{s(\eta_2) - s(\eta_1)}{t_2 - t_1}. \tag{7}$$

In this context, v denotes velocity, measured in meters per second (m/s), while t signifies time, expressed in seconds (s).

Upon substituting (6) into (7), we arrive at:

$$v(\eta) = \frac{\frac{2\pi r}{R}\eta_2 - \frac{2\pi r}{R}\eta_1}{t_2 - t_1}, \tag{8}$$

and after factorizing :

$$v(\eta) = \frac{2\pi r}{R}\left(\frac{\eta_2 - \eta_1}{t_2 - t_1}\right) = \frac{2\pi r}{R}\left(\frac{\Delta\eta}{\Delta t}\right). \tag{9}$$

A nine-axis Inertial Measurement Unit (IMU) equipped with RS485 communication is employed to precisely measure orientation, velocity, and gravitational force parameters. This IMU provides data from an accelerometer, gyroscope, and magnetometer into a cohesive output, providing insights into the module's dynamics.

Positioned at the termination point of the module's output link, as depicted in Figure 6, the IMU plays a pivotal role in determining angular and linear positions, as well as angular and linear velocities. Leveraging equations 1, 6, 4, and 8, respectively, the IMU facilitates accurate and real-time tracking of the module's motion parameters.

In combination, a planetary mechanism is utilized to model the output angle, allowing for the precise determination of linear displacement in conjunction with the encoder. Let ϕ_a represent the angle of the planetary system's ring gear, thereby inferring the displacement of the piston and enabling comprehensive analysis of the module's movements and dynamics.

$$s_p = \frac{L}{2}\left(\phi_a + \iint_t \hat{a}_{yaw} dt^2\right), \tag{10}$$

where the screw linear advance parameter is

$$L = \frac{N}{n}. \tag{11}$$

In this context, L stands for the advance in meters (m), N signifies the number of parallel strings, and n denotes the number of strings per linear metric unit.

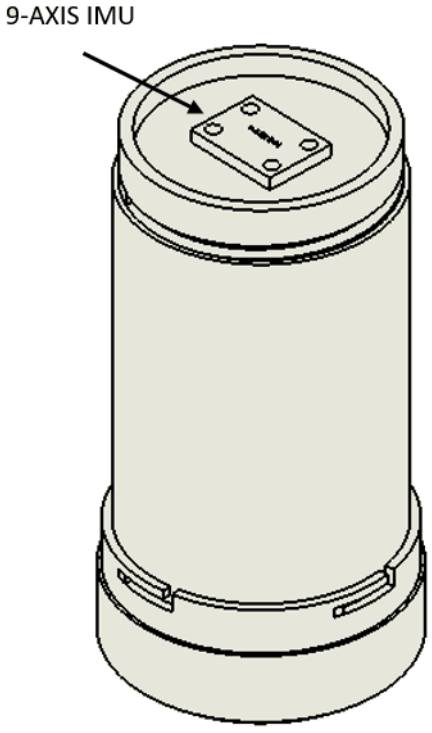

Figure 6: *Strategic positioning of the geometric measurement model with the 9-axis IMU.*

The connections of the three DC motors with encoders and the IMU are routed to an Arduino MEGA microcontroller. However, the rotational movement of the toothed sphere, coupled with the placement of the IMU and one of the DC motors inside it, raises concerns about cable entanglement. To effectively address this challenge, a rotary electrical connector is employed (rec). Positioned at the base of the sphere, as depicted in Figure 7, this connector comprises a fixed side

and a rotating side. The fixed side is housed within the toothed sphere, while the rotating side facilitates connections to both the exterior of the sphere and the microcontroller. This approach ensures communication while accommodating the dynamic movement of the mechanism.

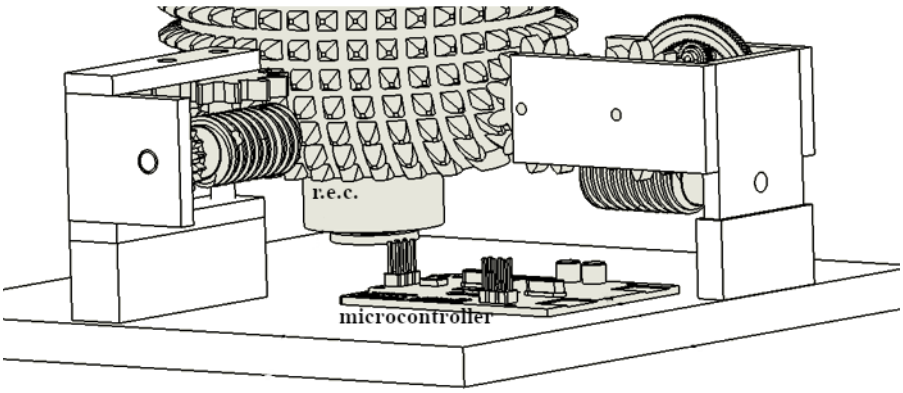

Figure 7: *Location of the rotary electrical connector to the interior motor of the spherical joint.*

At the module output, sensing of three dynamic variables along the pitch, yaw, and roll axes is crucial. These variables encompass position angle, velocity, and acceleration, measured respectively by an inclinometer, a gyroscope, and an accelerometer. The general models for the Euler angles of the link are as follows:

$$\phi_t = \left[\hat{\phi}_i + \int_t \hat{\dot{\phi}}_g dt + \iint_t \frac{\hat{a}_a}{dt} dt^2\right] \frac{1}{3}, \tag{12}$$

as well as Eulerian angular velocities:

$$\dot{\phi}_t = \left[\frac{d}{dt}\hat{\phi}_i + \dot{\phi}_g + \int_t \frac{\hat{a}}{dt} dt\right] \frac{1}{3}, \tag{13}$$

and the comprehensive inertial model of angular accelerations:

$$\ddot{\phi}_t = \left[\frac{d^2}{dt^2}\hat{\phi}_i + \frac{d}{dt}\hat{\dot{\phi}}_g + \frac{\hat{a}_a}{dt}\right] \frac{1}{3}. \tag{14}$$

In this context, ϕ_t, $\dot{\phi}_t$ and $\ddot{\phi}_t$ represent the estimator models, whereas $\hat{\phi}$, $\hat{\dot{\phi}}$, and $\hat{\ddot{\phi}}$ denote the direct sensor measurements.

5 Modular mechanism dynamics

In this section, we derive the dynamic modeling of the mechanisms within the modular device. We analyze the kinetic and potential energies obtained from the kinematic models, employing an Euler-Lagrange approach to develop the dynamic model.

Following the symbolic notation of mechanisms as introduced in the Mechanics course, for the purpose of this project, we establish the following definitions:

Definition 1 (Mechanism Notation)**.** *Let e_i represent a gear, g_i a worm screw, and Δ_i a planetary gear, interconnected in various ways: perpendicular, parallel, via belt, and serially.*

Thus, from Definition 1, we derive the representation of the pitch mechanism, outlined in the following Definition 2.

Definition 2 (Pitch Mechanism)**.** *Let e_0 denote the pinion of the actuator or global driving gear, meshed perpendicularly with e_1. Subsequently, with an axis collinear to g_2 and this to e_3. Then e_3 connected perpendicularly to Δ_4 and this connected again perpendicularly to e_5. Finally, e_5 is in serial connection to e_6.*

Similarly, for the yaw rotation mechanism, its mechanical connection is described using the following notation provided by Definition 3,

Definition 3 (Yaw Mechanism)**.** *Let e_{19} represent the pinion of the actuator (global driving gear) connected perpendicularly to e_{20}. Subsequently, e_{20} is connected in parallel to g_{21}, which transmits to e_{22}. Then, e_{22} is serially connected to e_{23}, and finally, it is connected in parallel to e_{24}.*

Essentially, considering the interconnection of mechanical elements formalizes the prismatic displacement mechanism described by the notation in Definition 4.

Definition 4 (Prismatic Mechanism)**.** *Let e_{29} represent the actuator pinion or global driving gear, connected in parallel to Δ_{30}, which is also parallel to Δ_{35}.*

Hence, Definitions 1, 2, 3, and 4, which delineate the physical systems, serve as the cornerstone for deriving the kinematic models in subsequent sections.

5.1 Kinematic Model

In this context, all mechanisms are established as underactuated systems, typically controlled by a single variable that operates independently, often facilitated by a global driving gear $e_0(\phi_0)$. Kinematic model of the pitch mechanism is deduced starting from (15) and resulting in expression (20), based on Figure 1.

$$\phi_1 = \left(-\frac{r_0}{r_1}\right)\phi_0, \tag{15}$$

and the connection of e_1 on a parallel face with g_2, both aligned along a collinear axis, signifies a gear transmission by parallel faces and a collinear axis. This configuration indicates that:

$$\phi_2 = \phi_1. \tag{16}$$

The coupling of g_2 and e_3 represents a worm gear connection, wherein:

$$\phi_3 = \left(-\frac{n_2}{n_3}\right)\phi_2 = \left(\frac{r_0 n_2}{r_1 n_3}\right)\phi_0. \tag{17}$$

Similarly, the collinear parallel axis connection between e_3 and the planetary gearing system Δ_4 (e_3 in parallel to Δ_4, denotes a direct parallel alignment of axes:

$$\phi_4 = \left(\frac{4r_{s4}^2}{(r_{s4}+r_{a4})^2}\right)\phi_3 = \left(\frac{4r_{s4}^2 r_0 n_2}{(r_{s4}+r_{a4})^2 r_1 n_3}\right)\phi_0, \tag{18}$$

and subsequently, the parallel connection between Δ_4 and e_5 is assumed,

$$\phi_5 = \phi_4. \tag{19}$$

Finally, building upon Definitions 1 and 4, the series connection e_5 - e_6 is elucidated by Proposition 1.

Proposition 1 (Pitch Rotation Gear)**.** *Leveraging the deductions from earlier motion transmissions, we derive the rotary model of ϕ_6. This model is subject to a mechanical advantage term intrinsic to the prior connection of mechanical elements, as depicted below:*

$$\phi_6 = -\frac{r_5}{r_6}\phi_5 = -\left(\frac{4r_{s4}^2 r_0 r_5 n_2}{(r_{s4}+r_{a4})^2 r_1 r_6 n_3}\right)\phi_0. \tag{20}$$

Such that r_i and n_i are defined by Definition 5.

Definition 5 (Gear-Worm Screw parameters)**.** *Let r_i denote the radii [m] of the respective e_i, and n_i represent the number of threads of g_i connected to the threads n_{i+1} of e_{i+1}.*

The kinematic model of the yaw mechanism begins (21) and results in Proposition (2). Firstly, there is a perpendicular connection between the driving gear e_{19} and gear e_{20} given by:

$$\phi_{20} = \left(-\frac{r_{19}}{r_{20}}\right)\phi_{19}, \tag{21}$$

and followed by a parallel, colinear shaft connection between gear e_{20} and worm gear g_{21}, where:

$$\phi_{21} = \phi_{20}. \tag{22}$$

Next, from Definition 5, the worm gear connection between g_{21} and e_{22} is given by:

$$\phi_{22} = \left(\frac{n_{21}}{n_{22}}\right)\phi_{21} = \left(-\frac{r_{19}n_{21}}{r_{20}n_{22}}\right)\phi_{19}. \tag{23}$$

The series connection between gears e_{22} and e_{23} is expressed as follows:

$$\phi_{23} = \left(-\frac{r_{22}}{r_{23}}\right)\phi_{22} = \left(\frac{r_{19}r_{22}n_{21}}{r_{20}r_{23}n_{22}}\right)\phi_{19}, \tag{24}$$

and there's the parallel collinear axis connection between e_{23} and e_{24},

$$\phi_{24} = \phi_{23}, \tag{25}$$

where the latter is given by Proposition 2.

Proposition 2 (Yaw Rotation Gear)**.** *Given the previous algebraic deductions, the kinematic rotary transmission model for gear ϕ_{24} is obtained, expressed as follows:*

$$\phi_{24} = \left(-\frac{r_{22}}{r_{23}}\right)\phi_{22} = \left(\frac{r_{19}r_{22}n_{21}}{r_{20}r_{23}n_{22}}\right)\phi_{19}. \tag{26}$$

In this context, r_i signifies the radii [m] of the corresponding e_i, while n_{21} represents the number of teeth on gear g_{21} engaged with the teeth n_{22} of gear e_{22}.

In the context of the kinematic model of the prismatic mechanism, the input ϕ_{29} transmits motion to the planetary system Δ_{30}. The planetary system Δ_{30} is characterized by transmitting output motion via a carrier. The velocity at the output (carrier) of Δ_{30} in such a planetary system is derived from the following motion relationship:

$$v_s = \frac{p_c}{p_s}v_c. \tag{27}$$

In this equation, v_s represents the speed of the sun gear, p_c denotes the perimeter of the carrier, and p_s stands for the perimeter of the sun gear. Consequently, the tangential velocity of the sun gear progresses at a rate of $\frac{P_c}{P_s}$ times the tangential velocity along the circumferential path of the carrier. Here, P_c and P_s signify the perimeters of the carrier and the sun gear, respectively. Knowing that $v_s = r_s\omega_s$ and $v_c = r_c\omega_c$, we can substitute these expressions into (27),

$$r_s\omega_s = \frac{2\pi r_c}{2\pi r_s} r_c\omega_c, \tag{28}$$

where $r_c = \frac{r_a - r_s}{2} + r_s$. Hence

$$r_s\omega_s = \left(\frac{\frac{r_a-r_s}{2} + r_s}{r_s}\right)\left(\frac{r_a - r_s}{2} + r_s\right)\omega_c = \frac{(r_s + r_a)^2}{4r_s}\omega_c, \tag{29}$$

and solving for ω_c, where $\omega_c = \phi_{c30}$ and $\omega_s = \phi_{s30} = \phi_{29}$, we find:

$$\phi_{c30} = \frac{4r_s^2}{(r_s + r_a)^2}\phi_{29}. \tag{30}$$

Hence, the output model on the carrier of the second planetary system is as follows:

$$\phi_{c35} = \frac{4r_s^2}{(r_s + r_a)^2}\phi_{c30}. \tag{31}$$

Substituting (30), we have the following proposition:

Proposition 3 (Prismatic Rotation Gear)**.** *Based on previous algebraic deductions, the rotation model ϕ_{35} preceded by the two cascaded planetary gears is proposed, such that its kinematic model is expressed as:*

$$\phi_{c35} = \left(\frac{4r_s^2}{(r_s + r_a)^2}\right)\left(\frac{4r_s^2}{(r_s + r_a)^2}\phi_{29}\right) = \frac{16r_s^4}{(r_s + r_a)^4}\phi_{29} \tag{32}$$

Where r_a represents the radius of the planetary system's ring. The displacement d_{T35} of the screw-type prismatic link is determined by:

$$d_{T36} = L\phi_{c35} \tag{33}$$

Where $L = Np$, where N represents the number of strings and p denotes the pitch or advancement parameter, $\frac{1}{n}$. Thus,

$$d_{T36} = L\left(\frac{16r_s^4}{(r_s + r_a)^4}\phi_{29}\right) \tag{34}$$

5.2 Dynamic Model

By formulating the Lagrangian operators consistent with the motion geometry outlined by the preceding kinematic models, our objective is to derive the dynamic model for each component of the pitch mechanism. Given that energy transmission takes place through a tooth of each gear, whose height varies periodically, we arrive at the following energy equation for each individual gear:

$$\mathscr{L}_0 = \frac{1}{2}I_0\dot{\phi}_0^2 - m_0 g r_0 \sin(\phi_0), \tag{35}$$

$$\mathscr{L}_1 = \frac{1}{2} I_1 \dot{\phi}_1^2 - m_1 g r_1 \sin(\phi_1), \tag{36}$$

$$\mathscr{L}_2 = \frac{1}{2} I_2 \dot{\phi}_2^2 - m_2 g r_2 \sin(\phi_2), \tag{37}$$

$$\mathscr{L}_3 = \frac{1}{2} I_3 \dot{\phi}_3^2 - m_3 g r_3 \sin(\phi_3), \tag{38}$$

$$\mathscr{L}_4 = \frac{1}{2} I_4 \dot{\phi}_4^2 - m_4 g r_4 \sin(\phi_4), \tag{39}$$

$$\mathscr{L}_5 = \frac{1}{2} I_5 \dot{\phi}_5^2 - m_5 g r_5 \sin(\phi_5), \tag{40}$$

$$\mathscr{L}_6 = \frac{1}{2} I_6 \dot{\phi}_6^2 - m_6 g r_6 \sin(\phi_6). \tag{41}$$

Hereafter, we may define the Langrangian vector $\vec{\mathscr{L}} = (\mathscr{L}_0, \ldots, \mathscr{L}_6)^\top$ to be used by following Definition 6.

Definition 6 (Energy Model of the Pitch Mechanism)**.** *Let $\mathscr{L}_i$ denote the Lagrangian operator for each element constituting the pitch mechanism. This operator accounts for both the rotational kinetic energy and the potential energy transmitted by a tooth of the preceding gear to the subsequent gear. The set of energy differentials is defined as:*

$$\vec{\mathscr{L}} = \frac{1}{2} \begin{pmatrix} I_0 & 0 & 0 & 0 & 0 & 0 & 0 \\ 0 & I_1 & 0 & 0 & 0 & 0 & 0 \\ 0 & 0 & I_2 & 0 & 0 & 0 & 0 \\ 0 & 0 & 0 & I_3 & 0 & 0 & 0 \\ 0 & 0 & 0 & 0 & I_4 & 0 & 0 \\ 0 & 0 & 0 & 0 & 0 & I_5 & 0 \\ 0 & 0 & 0 & 0 & 0 & 0 & I_6 \end{pmatrix} \begin{pmatrix} \dot{\phi}_0 \\ \dot{\phi}_1 \\ \dot{\phi}_2 \\ \dot{\phi}_3 \\ \dot{\phi}_4 \\ \dot{\phi}_5 \\ \dot{\phi}_6 \end{pmatrix}^2 - \begin{pmatrix} m_0 g r_0 & 0 & 0 & 0 & 0 & 0 & 0 \\ 0 & m_1 g r_1 & 0 & 0 & 0 & 0 & 0 \\ 0 & 0 & m_2 g r_2 & 0 & 0 & 0 & 0 \\ 0 & 0 & 0 & m_3 g r_3 & 0 & 0 & 0 \\ 0 & 0 & 0 & 0 & m_4 g r_4 & 0 & 0 \\ 0 & 0 & 0 & 0 & 0 & m_5 g r_5 & 0 \\ 0 & 0 & 0 & 0 & 0 & 0 & m_6 g r_6 \end{pmatrix} \begin{pmatrix} \sin(\phi_0) \\ \sin(\phi_1) \\ \sin(\phi_2) \\ \sin(\phi_3) \\ \sin(\phi_4) \\ \sin(\phi_5) \\ \sin(\phi_6) \end{pmatrix}, \tag{42}$$

where I_i is the moment of inertia, ϕ_i and $\dot{\phi}_i$ represent the rotation angle and velocity, respectively, m_i is the mass of the gear, and g denotes gravitational force. Alternatively, the abbreviated form of the preceding Lagrangian vector in this definition is established as follows:

$$\vec{\mathscr{L}} = \mathbf{M}\dot{\phi}^2 - \mathbf{G}\mathbf{g}(\Phi). \tag{43}$$

For the sake of clarity, when solving each mechanical element separately using the Lagrangian equations as outlined in Definition 6, let's address the Euler-Lagrange differential equation according to the following expressions:

$$\frac{\partial \vec{\mathscr{L}}}{\partial \Phi} = \frac{d}{dt} \left(\frac{\partial \vec{\mathscr{L}}}{\partial \dot{\Phi}_i} \right). \tag{44}$$

In the case of all elements e_i undergoing rotational motion, we calculate the torques exerted on each element individually, considering their respective rotational dynamics and interactions within the system. This comprehensive analysis allows us to discern and quantify the rotational forces acting on each element, providing valuable insights into the system's overall mechanical behavior. For the global conductor pinion, the dynamic expression is

$$\tau_0 = \frac{du}{dt}\left(I_0\dot{\phi}_0\right) + m_0 g r_0 \cos(\phi_0) = I_0\ddot{\phi} + m_0 g r_0 \cos(\phi_0). \tag{45}$$

Subsequently, for gear e_1,

$$\tau_1 = \frac{du}{dt}\left(I_1\dot{\phi}_1\right) + m_1 g r_1 \cos(\phi_1) = I_1\ddot{\phi} + m_1 g r_1 \cos(\phi_1), \tag{46}$$

when we substitute ϕ_1 from equation (15), we obtain the following:

$$\tau_1 = I_1\left(-\frac{r_0}{r_1}\right)\ddot{\phi}_0 + m_1 g r_1 \cos\left(-\frac{r_0}{r_1}\phi_0\right). \tag{47}$$

Likewise,

$$\tau_2 = \frac{du}{dt}\left(I_2\dot{\phi}_2\right) + m_2 g r_2 \cos(\phi_2) = I_2\ddot{\phi}_2 + m_2 g r_2 \cos(\phi_2), \tag{48}$$

when we substitute ϕ_2 from equation (16), we obtain the following:

$$\tau_2 = I_2\left(-\frac{r_0}{r_1}\right)\ddot{\phi}_0 + m_2 g r_2 \cos\left(-\frac{r_0}{r_1}\phi_0\right). \tag{49}$$

Similarly,

$$\tau_3 = \frac{du}{dt}\left(I_3\dot{\phi}_3\right) - \left(-m_3 g r_3 \cos(\phi_3)\right) = I_3\ddot{\phi}_3 + m_3 g r_3 \cos(\phi_3), \tag{50}$$

where upon substituting ϕ_3 from equation (17), we obtain the following:

$$\tau_3 = I_3\left(\frac{r_0 n_2}{r_1 n_3}\right)\ddot{\phi}_0 + m_3 g r_3 \cos\left(\frac{r_0 n_2}{r_1 n_3}\phi_0\right). \tag{51}$$

Subsequently,

$$\tau_4 = \frac{du}{dt}\left(I_4\dot{\phi}_4\right) - \left(-m_4 g r_4 \cos(\phi_4)\right) = I_4\ddot{\phi}_4 + m_4 g r_4 \cos(\phi_4), \tag{52}$$

and substituting ϕ_4 into equation (18), we get the following:

$$\tau_4 = I_4\left(\frac{4r_{s4}^2 r_0 n_2}{(r_{s4}+r_{a4})^2 r_1 n_3}\right)\ddot{\phi}_0 + m_4 g r_4 \cos\left(\frac{4r_{s4}^2 r_0 n_2}{(r_{s4}+r_{a4})^2 r_1 n_3}\phi_0\right). \tag{53}$$

Thus, for τ_5,

$$\tau_5 = \frac{du}{dt}\left(\frac{2}{2}I_5\dot{\phi}_5\right) - \left(-m_5 g r_5 \cos(\phi_5)\right) = I_5\ddot{\phi}_5 + m_5 g r_5 \cos(\phi_5), \tag{54}$$

and substituting ϕ_5 into equation (19), we obtain the following:

$$\tau_5 = I_5\left(\frac{4r_{s4}^2 r_0 n_2}{(r_{s4}+r_{a4})^2 r_1 n_3}\right)\ddot{\phi}_0 + m_5 g r_5 \cos\left(\frac{4r_{s4}^2 r_0 n_2}{(r_{s4}+r_{a4})^2 r_1 n_3}\phi_0\right). \tag{55}$$

Finally, for τ_6,

$$\tau_6 = \frac{du}{dt}\left(\frac{2}{2} I_6 \dot{\phi}_6\right) - (-m_6 g r_6 \cos(\phi_6)) = I_6 \ddot{\phi}_6 + m_6 g r_6 \cos(\phi_6), \tag{56}$$

when we substitute ϕ_6 into equation (20), we obtain the following:

$$\tau_6 = I_6 \left(-\frac{4 r_{s4}^2 r_0 r_5 n_2}{(r_{s4}+r_{a4})^2 r_1 r_6 n_3}\right) \ddot{\phi}_0 + m_6 g r_6 \cos\left(-\frac{4 r_{s4}^2 r_0 r_5 n_2}{(r_{s4}+r_{a4})^2 r_1 r_6 n_3} \phi_0\right). \tag{57}$$

Theorem 1 (Pitch mechanism torque)**.** *The differential equation governing the total system of the pitch mechanism results in a second-order nonlinear differential equation, for which finding an analytical solution is nontrivial. Hence, the following law of dynamics for the mechanical system establishes $\tau\left(\ddot{\phi}_0, \phi_0\right)$ for all simultaneous elements of the pitch controlled by the same independent control variables. It is expressed as follows:*

$$\begin{bmatrix} \tau_0 \\ \tau_1 \\ \tau_2 \\ \tau_3 \\ \tau_4 \\ \tau_5 \\ \tau_6 \end{bmatrix} = \begin{bmatrix} I_0 \\ -I_1 \frac{r_0}{r_1} \\ -I_2 \frac{r_0}{r_1} \\ I_3 \frac{r_0 n_2}{r_1 n_3} \\ 4 I_4 \frac{r_{s4}^2 r_0 n_2}{(r_{s4}+r_{a4})^2 r_1 n_3} \\ 4 I_5 \frac{r_{s4}^2 r_0 n_2}{(r_{s4}+r_{a4})^2 r_1 n_3} \\ -4 I_6 \frac{r_{s4}^2 r_0 r_5 n_2}{(r_{s4}+r_{a4})^2 r_1 r_6 n_3} \end{bmatrix} \ddot{\phi}_0 + \begin{bmatrix} m_0 r_0 \cos(\phi_0) \\ m_1 r_1 \cos(-\frac{r_0}{r_1}\phi_0) \\ m_2 r_2 \cos(-\frac{r_0}{r_1}\phi_0) \\ m_3 r_3 \cos(-\frac{r_0 n_2}{r_1 n_3}\phi_0) \\ m_4 r_4 \cos(K_{\Delta 4}\frac{r_0 n_2}{r_1 n_3}\phi_0) \\ m_5 r_5 \cos(K_{\Delta 4}\frac{r_0 n_2}{r_1 n_3}\phi_0) \\ m_6 r_6 \cos(K_{\Delta 4}\frac{r_0 r_5 n_2}{r_1 r_6 n_3}\phi_0) \end{bmatrix} g. \tag{58}$$

Similarly

$$K_{\Delta 4} = \frac{r_{s4}^2}{(r_{s4}+r_{a4})^2} \tag{59}$$

Where $K_{\Delta 4}$ is the mechanical advantage given by the relationship between r_s and r_a.

Formulating the Lagrangian operators according to the motion geometry established by the kinematic models of the yaw mechanism, we derive the following Definition 7.

Definition 7 (Yaw mechanism energy model)**.** *Let $\mathscr{L}_i$ represent the Lagrangian operator for each element comprising the yaw mechanism. This operator considers both the rotational kinetic energy and the potential energy transmitted by a tooth of the preceding gear to the subsequent gear. The set of energy differentials is defined as:*

$$\mathscr{L}_{19} = \frac{1}{2} I_{19} \dot{\phi}_{19}^2 - m_{19} g r_{19} \sin(\phi_{19}) \tag{60}$$

$$\mathscr{L}_{20} = \frac{1}{2} I_{20} \dot{\phi}_{20}^2 - m_{20} g r_{20} \sin(\phi_{20}) \tag{61}$$

$$\mathscr{L}_{21} = \frac{1}{2} I_{21} \dot{\phi}_{21}^2 - m_{21} g r_{21} \sin(\phi_{21}) \tag{62}$$

$$\mathscr{L}_{22} = \frac{1}{2} I_{22} \dot{\phi}_{21}^2 - m_{22} g r_{22} \sin(\phi_{22}) \tag{63}$$

$$\mathscr{L}_{23} = \frac{1}{2} I_{23} \dot{\phi}_{23}^2 - m_{23} g r_{23} \sin(\phi_{23}) \tag{64}$$

$$\mathscr{L}_{24} = \frac{1}{2} I_{24} \dot{\phi}_{24}^2 - m_{24} g r_{24} \sin(\phi_{24}) \tag{65}$$

By applying the same analytical method used in the previous analysis of the pitch mechanisms, and subsequently solving the Lagrangian equations, we obtain the torques for each element.

$$\tau_{19} = \frac{d}{dt}\left(I_{19}\dot{\phi}_{19}\right) + m_{19}gr_{19}\cos(\phi_{19}) = I_{19}\ddot{\phi}_{19} + m_{19}gr_{19}\cos(\phi_{19}). \tag{66}$$

Likewise,

$$\tau_{20} = \frac{d}{dt}\left(I_{20}\dot{\phi}_{20}\right) + m_{20}gr_{20}\cos(\phi_{20}) = I_{20}\ddot{\phi}_{20} + m_{20}gr_{20}\cos(\phi_{20}), \tag{67}$$

when substituting ϕ_{20} into equation (21), we obtain:

$$\tau_{20} = I_{20}\left(-\frac{r_{19}}{r_{20}}\right)\ddot{\phi}_{19} + m_{20}gr_{20}\cos\left(-\frac{r_{19}}{r_{20}}\phi_{19}\right). \tag{68}$$

Moreover,

$$\tau_{21} = \frac{d}{dt}\left(I_{21}\dot{\phi}_{21}\right) + m_{21}gr_{21}\cos(\phi_{21}) = I_{21}\ddot{\phi}_{21} + m_{21}gr_{21}\cos(\phi_{21}), \tag{69}$$

and substituting ϕ_{21} into equation (22),

$$\tau_{21} = I_{21}\left(-\frac{r_{19}}{r_{20}}\right)\ddot{\phi}_{19} + m_{21}gr_{21}\cos\left(-\frac{r_{19}}{r_{20}}\phi_{19}\right). \tag{70}$$

Furthermore,

$$\tau_{22} = \frac{d}{dt}\left(I_{22}\dot{\phi}_{22}\right) - \left(-m_{22}gr_{22}\cos(\phi_{22})\right) = I_{22}\ddot{\phi}_{22} + m_{22}gr_{22}\cos(\phi_{22}), \tag{71}$$

when substituting ϕ_{22} into equation (23),

$$\tau_{22} = I_{22}\left(-\frac{r_{19}n_{21}}{r_{20}n_{22}}\right)\ddot{\phi}_{19} + m_{22}gr_{22}\cos\left(-\frac{r_{19}n_{21}}{r_{20}n_{22}}\phi_{19}\right). \tag{72}$$

$$\tau_{23} = \frac{d}{dt}\left(I_{23}\dot{\phi}_{23}\right) - \left(-m_{23}gr_{23}\cos(\phi_{23})\right) = I_{23}\ddot{\phi}_{23} + m_{23}gr_{23}\cos(\phi_{23}), \tag{73}$$

when we substitute ϕ_{23} into equation (24),

$$\tau_{23} = I_{23}\left(\frac{r_{19}r_{22}n_{21}}{r_{20}r_{23}n_{22}}\right)\ddot{\phi}_{19} + m_{23}gr_{23}\cos\left(\frac{r_{19}r_{22}n_{21}}{r_{20}r_{23}n_{22}}\phi_{19}\right). \tag{74}$$

Finally,

$$\tau_{24} = \frac{d}{dt}\left(I_{24}\dot{\phi}_{24}\right) - \left(-m_{24}gr_{24}\cos(\phi_{24})\right) = I_{24}\ddot{\phi}_{24} + m_{24}gr_{24}\cos(\phi_{24}), \tag{75}$$

and substituting ϕ_{24} into equation (26) to obtain

$$\tau_{24} = I_{24}\left(\frac{r_{19}r_{22}n_{21}}{r_{20}r_{23}n_{22}}\right)\ddot{\phi}_{19} + m_{24}gr_{24}\cos\left(\frac{r_{19}r_{22}n_{21}}{r_{20}r_{23}n_{22}}\phi_{19}\right). \tag{76}$$

Theorem 2 (Yaw mechanism torque)**.** *The differential equation describing the total system of the yaw mechanism results in a second-order nonlinear differential equation, for which finding an analytical solution is nontrivial. Hence, the following law of dynamics for the mechanical system establishes* $\tau\left(\ddot{\phi}_0, \phi_0\right)$ *for all simultaneous elements of the yaw controlled by the same independent control variables, and it is expressed as follows:*

$$\begin{bmatrix} \tau_{19} \\ \tau_{20} \\ \tau_{21} \\ \tau_{22} \\ \tau_{23} \\ \tau_{24} \end{bmatrix} = \begin{bmatrix} I_{19} \\ I_{20}\left(-\frac{r_{19}}{r_{20}}\right) \\ I_{21}\left(-\frac{r_{19}}{r_{20}}\right) \\ I_{22}\left(-\frac{r_{19}n_{21}}{r_{20}n_{22}}\right) \\ I_{23}\left(\frac{r_{19}r_{22}n_{21}}{r_{20}r_{23}n_{22}}\right) \\ I_{24}\left(\frac{r_{19}r_{22}n_{21}}{r_{20}r_{23}n_{22}}\right) \end{bmatrix} \ddot{\phi}_{19} + \begin{bmatrix} m_{19}r_{19}\cos(\phi_{19}) \\ m_{20}r_{20}\cos\left(-\frac{r_{19}}{r_{20}}\phi_{19}\right) \\ m_{21}r_{21}\cos\left(-\frac{r_{19}}{r_{20}}\phi_{19}\right) \\ m_{22}r_{22}\cos\left(-\frac{r_{19}n_{21}}{r_{20}n_{22}}\phi_{19}\right) \\ m_{23}r_{23}\cos\left(\frac{r_{19}r_{22}n_{21}}{r_{20}r_{23}n_{22}}\phi_{19}\right) \\ m_{24}r_{24}\cos\left(\frac{r_{19}r_{22}n_{21}}{r_{20}r_{23}n_{22}}\phi_{19}\right) \end{bmatrix} g. \tag{77}$$

Definition 8 (Prismatic Mechanism Energy Model)**.** *Let* $\mathscr{L}_{29}$ *denote the Lagrangian operator for each element of the prismatic mechanism, accounting for its rotational kinetic energy, as well as the potential energy transmitted from one gear tooth to the subsequent gear. The kinetic models are defined as:*

$$\mathscr{L}_{29} = \frac{1}{2}I_{29}\dot{\phi}_{29}^2 - m_{29}gr_{29}\sin(\phi_{29}) \tag{78}$$

$$\mathscr{L}_{c30} = \frac{1}{2}I_{c30}\dot{\phi}_{c30}^2 - m_{c30}gr_{c30}\sin(\phi_{c30}) \tag{79}$$

$$\mathscr{L}_{c35} = \frac{1}{2}I_{c35}\dot{\phi}_{c35}^2 - m_{c35}gr_{c35}\sin(\phi_{c35}) \tag{80}$$

$$\mathscr{L}_{T36} = \frac{1}{2}m_{T36}\dot{d}_{T36}^2 - m_{T36}gd_{T36} \tag{81}$$

Upon solving the previously presented equations, we derive the torque values for each individual element:

$$\tau_{29} = \frac{du}{dt}\left(I_{29}\dot{\phi}_{29}\right) + m_{29}gr_{29}\cos(\phi_{29}) = I_{29}\ddot{\phi}_{29} + m_{29}gr_{29}\cos(\phi_{29}), \tag{82}$$

as well as

$$\tau_{c30} = \frac{du}{dt}\left(I_{c30}\dot{\phi}_{c30}\right) - \left(-m_{c30}gr_{c30}\cos(\phi_{c30})\right) = I_{c30}\ddot{\phi}_{c30} + m_{c30}gr_{c30}\cos(\phi_{c30}), \tag{83}$$

upon substituting ϕ_{c30} into equation (30), we derive the following expression:

$$\tau_{c30} = I_{c30}\frac{4r_s^2}{\left(r_s + r_a\right)^2}\ddot{\phi}_{29} + m_{c30}gr_{c30}\cos\left(\frac{4r_s^2}{\left(r_s + r_a\right)^2}\phi_{29}\right). \tag{84}$$

Subsequently,

$$\tau_{c35} = \frac{du}{dt}\left(I_{c35}\dot{\phi}_{c35}\right) - \left(-m_{c35}gr_{c35}\cos(\phi_{c35})\right) = I_{c35}\ddot{\phi}_{c35} + m_{c35}gr_{c35}cos\left(\phi_{c35}\right), \tag{85}$$

where by substituting ϕ_{35} into equation (32), we derive the following:

$$\tau_{c35} = I_{c35}\frac{16r_s^4}{\left(r_s + r_a\right)^4}\ddot{\phi}_{c29} + m_{c35}gr_{c35}cos\left(\frac{16r_s^4}{\left(r_s + r_a\right)^4}\phi_{29}\right). \tag{86}$$

Finally,

$$f_{T36} = m_{T36}\ddot{d}_{T36} - m_{T36}g = m_{T36}L\left(\frac{16r_s^4}{\left(r_s + r_a\right)^4}\right)\ddot{\phi}_{29} - m_{T36}g \tag{87}$$

Theorem 3 (Torques and force of the prismatic mechanism)**.** *The differential equation governing the entire prismatic mechanism system leads to a second-order nonlinear differential equation, the analytical solution of which presents a nontrivial challenge. Consequently, the following law of mechanical system dynamics defines* $\tau\left(\ddot{\phi}_0, \phi_0\right)$ *for all simultaneously pitch-controlled elements using the same independent control variables, as expressed below:*

$$\begin{bmatrix} \tau_{29} \\ \tau_{c30} \\ \tau_{c35} \\ f_{T36} \end{bmatrix} = \begin{bmatrix} I_{29} \\ I_{c30}\left(\frac{4r_s^2}{(r_s+r_a)^2}\right) \\ I_{c35}\left(\frac{16r_s^4}{(r_s+r_a)^4}\right) \\ 0 \end{bmatrix} \ddot{\phi}_{29} + \begin{bmatrix} m_{29} r_{29} \cos(\phi_{29}) \\ m_{c30} r_{c30} \cos\left(\frac{4r_s^2}{(r_s+r_a)^2}\phi_{29}\right) \\ m_{c35} r_{c35} \cos\left(\frac{16r_s^4}{(r_s+r_a)^4}\phi_{29}\right) \\ m_{T36} L\left(\frac{16r_s^4}{(r_s+r_a)^4}\phi_{29}\right) \end{bmatrix} g. \tag{88}$$

6 Control module model

In this section, we present a kinematic control model for the module, employing variational methods to regulate the motion of coordinates with respect to all independent control variables (angular). From this framework, laws governing the control of joint variables are derived.

The position model deals with the coordinates of the module's link within the workspace. Its representation relies on the instantaneous variation of joint variables: yaw, pitch, and elongation. Referring to the reference system illustrated in Figure 5b, the pitch angle corresponds to rotation around the x-axis, while yaw variation of the module is linked to rotation around the z-axis. Additionally, the prismatic elongation of the module's link is denoted by d_t. Through analytical deduction of the system's geometry, Definition 9 is established using spherical coordinates.

Definition 9. *(Position Model) Let x, y, and z represent the coordinates in the workspace, and let A be the projection of* d_t *onto the xy plane. The following spherical model relies on the three joint variables* θ_0*,* θ_1*, and* d_t*, such that*

$$x = A\cos(\theta_0) = d_{T36}\cos(\theta_0)\cos(\theta_1), \tag{89}$$

likewise,

$$y = A\sin(\theta_0) = d_{T36}\sin(\theta_0)\cos(\theta_1), \tag{90}$$

and

$$z = d_{T36}\sin(\theta_1)). \tag{91}$$

Here, the term $A = d_{T36}\cos(\theta_1)$ *denotes the projection in meters.*

Derived from Definition 9, Proposition 4 intricately formulates the module's position model, leveraging the nuanced functional attributes of the gears.

Proposition 4. *(Intrinsic Variables Model) The coordinates in the workspace are directly dictated by the intrinsic variables of the modular mechanism, establishing a fundamental relationship between the system's internal parameters and its spatial positioning.*

$$\theta_0 = \phi_{24} = \left(\frac{r_{19} r_{22} n_{21}}{r_{20} r_{23} n_{22}}\right)\phi_{19}, \tag{92}$$

$$\theta_1 = \phi_6 = -\left(\frac{4r_{s4}^2 r_0 r_5 n_2}{(r_{s4}+r_{a4})^2 r_1 r_6 n_3}\right)\phi_0 \tag{93}$$

and

$$d_{T36} = L\left(\frac{16r_s^4}{(r_s+r_a)^4}\right)\phi_{29} \tag{94}$$

Hence, upon substituting θ_0, θ_1, and d_{T36} into the previously formulated equations, we obtain the following expressions:

$$x = A\cos(\theta_0) = L\left(\frac{16r_s^4}{(r_s+r_a)^4}\phi_{29}\right)\cos\left(\frac{r_{19}r_{22}n_{21}}{r_{20}r_{23}n_{22}}\phi_{19}\right)\cos\left(-\frac{4r_{s4}^2 r_0 r_5 n_2}{(r_{s4}+r_{a4})^2 r_1 r_6 n_3}\phi_0\right), \tag{95}$$

likewise,

$$y = A\sin(\theta_0) = L\left(\frac{16r_s^4}{(r_s+r_a)^4}\phi_{29}\right)\sin\left(\frac{r_{19}r_{22}n_{21}}{r_{20}r_{23}n_{22}}\phi_{19}\right)\cos\left(-\frac{4r_{s4}^2 r_0 r_5 n_2}{(r_{s4}+r_{a4})^2 r_1 r_6 n_3}\phi_0\right), \tag{96}$$

and

$$z = d_{T36}\sin(\theta_1) = L\left(\frac{16r_s^4}{(r_s+r_a)^4}\phi_{29}\right)\sin\left(-\frac{4r_{s4}^2 r_0 r_5 n_2}{(r_{s4}+r_{a4})^2 r_1 r_6 n_3}\phi_0\right). \tag{97}$$

Let $\mathbf{p} \in \mathbb{R}^3$ be defined as $\mathbf{p} = (x,y,z)^T$, and let $\dot{\mathbf{p}} = (\dot{x},\dot{y},\dot{z})^T$ represent the vector of Cartesian velocities tangent to the module's link. Define $\Phi = (\theta_0,\theta_1,d_t)^T$ such that the angular velocities are denoted by $\dot{\Phi} = (\dot{\theta}_0,\dot{\theta}_1,\dot{d_t})^T$. Based on the XYZ position model, the Jacobian matrix describing the evolution of all coordinates with respect to all independent control variables simultaneously is deduced as follows:

$$\mathbf{J}_t = \begin{bmatrix} -d_{T36}\sin(\theta_0)\cos(\theta_1) & d_{T36}\cos(\theta_0)\cos(\theta_1) & \cos(\theta_0)\cos(\theta_1) \\ d_{T36}\cos(\theta_0)\cos(\theta_1) & -d_{T36}\sin(\theta_0)\sin(\theta_1) & \sin(\theta_0)\cos(\theta_1) \\ 0 & d_{T36}\cos(\theta_1) & \sin(\theta_1) \end{bmatrix}. \tag{98}$$

It is characterized by its non-singular and invertible nature, this square matrix is also non-stationary.

Proposition 5. *(Kinematic Law) The relationship between Cartesian velocities and joint variables is expressed as a time-varying linear system. The gain for multiple outputs relative to multiple inputs is applicable in the direct solution model.*

$$\begin{bmatrix} \dot{x} \\ \dot{y} \\ \dot{z} \end{bmatrix} = \mathbf{J}_t \begin{bmatrix} \dot{\theta}_0 \\ \dot{\theta}_1 \\ \dot{d}_{T36} \end{bmatrix}. \tag{99}$$

Likewise, the inverse model

$$\begin{bmatrix} \dot{\theta}_0 \\ \dot{\theta}_1 \\ \dot{d}_{T36} \end{bmatrix} = \mathbf{J}_t^{-1} \cdot \begin{bmatrix} \dot{x} \\ \dot{y} \\ \dot{z} \end{bmatrix} \tag{100}$$

and defining the vector of module's joint variables as $\dot{\Theta} = \left(\dot{\theta}_0,\dot{\theta}_1,\dot{d}_{T36}\right)^T$, and the vector of Cartesian variables in the workspace as $\dot{\mathbf{p}} = (\dot{x},\dot{y},\dot{z})^T$.

6.1 Kinematic Control Law

Based on Proposition 5, which encapsulates the direct and inverse kinematic laws of the proposed module in a single equation, the direct solution in terms of its first-order derivative is:

$$\dot{\mathbf{p}} = \mathbf{J}_t \cdot \dot{\Theta}. \tag{101}$$

Expressing it as a first-order linear differential equation, we can solve it using the method of separation of variables and derivatives with respect to dt, as follows:

$$\frac{\mathrm{d}\mathbf{p}}{\mathrm{d}t} = \mathbf{J_t} \cdot \frac{\mathrm{d}\Theta}{\mathrm{d}t}, \tag{102}$$

when integrating with respect to both differentials,

$$\int_{\mathbf{p_t}}^{\mathbf{p}_{t+1}} d\mathbf{P} = \mathbf{J} \cdot \int_{\Theta_t}^{\Theta_{t+1}} d\Theta, \tag{103}$$

This leads to a recursive expression. Drawing from Proposition 5 as a foundational element, Theorem 4 is articulated as follows.

Theorem 4. *(Kinematic control law) The theorem articulates the control law, which governs both the degrees of freedom and the control joint variables, as established by*

$$\mathbf{p_{t+1}} - \mathbf{p_t} = \mathbf{J} \cdot (\Theta_{t+1} - \Theta_t). \tag{104}$$

Where, (I) below, denotes the initial position control law employing the joint variables as input references, with the direct kinematic controller being

(i)

$$\mathbf{p}_{t+1} = \mathbf{p}_t + \mathbf{J}\left(\Theta^{ref} - \hat{\Theta}_t\right), \tag{105}$$

and (II) signifies the control law for the joint variables, where Cartesian position serves as the global reference for the prismatic link, and the inverse kinematic controller is employed.

(ii)

$$\Theta_{t+1} = \Theta_t + \mathbf{J}^{-1}\left(\mathbf{p}^{ref} - \hat{\mathbf{p}}_t\right). \tag{106}$$

By iteratively employing both expressions, feedback errors are progressively diminished through successive approximations.

$$\mathbf{p_{t+1}} = \mathbf{p_t} + \mathbf{J}_t \cdot (\Theta_{t+1} - \Theta_t) \tag{107}$$

$$\Theta_{t+1} = \Theta_t + \mathbf{J}_t^{-1} \cdot \left(\mathbf{p^{ref}} - \mathbf{p}_t\right). \tag{108}$$

Thus, the Jacobian $\mathbf{J}(\Theta_{t+1})$ will be continuously updated in each subsequent iteration until the desired Cartesian reference position satisfies the condition $||\mathbf{p}^{ref} - \hat{\mathbf{p}}_t|| < \varepsilon$.

7 Robotic Reconfigurations

7.1 Two-wheel reconfiguration

A 2W2D robot, short for a two-wheel two-drive robot, is characterized by its configuration featuring 2 wheels and 2 drive units. This configuration enables each wheel to operate independently, granting the robot a high degree of maneuverability and versatility. As illustrated in Figure 8, each module comprising the vehicle is equipped with two distinct wheels, allowing for agile and dynamic movement across various terrains and environments. The instantaneous velocity of the mobile robot is calculated based on the rotational speeds of its individual wheels. Specifically,

the velocity of the right wheel (V_R) and the velocity of the left wheel (V_L) are determined by the product of the wheel radius (r) and the respective angular velocities ($\dot{\phi}_R$ and $\dot{\phi}_L$). This relationship encapsulates how the robot's motion is directly influenced by the rotation of its wheels, crucial for navigation and control in diverse operational scenarios.

$$v = \frac{1}{2}(v_R + v_L) \tag{109}$$

Where V_R represents the velocity of the right wheel, determined by $r \cdot \dot{\phi}_R$, and V_L denotes the velocity of the left wheel, expressed as $r \cdot \dot{\phi}_L$. This yields the velocity in terms of the wheels' rotation:

$$v = \frac{r}{2}\dot{\phi}_R + \frac{r}{2}\dot{\phi}_L \tag{110}$$

and the vehicular robot's angular velocity is given by:

$$\omega = \frac{2r}{b}\left(\dot{\phi}_R - \dot{\phi}_L\right) = \frac{2r}{b}\dot{\phi}_R - \frac{2r}{b}\dot{\phi}_L \tag{111}$$

where b is the distance between the left wheel and the right wheel, as depicted in Figure 8.

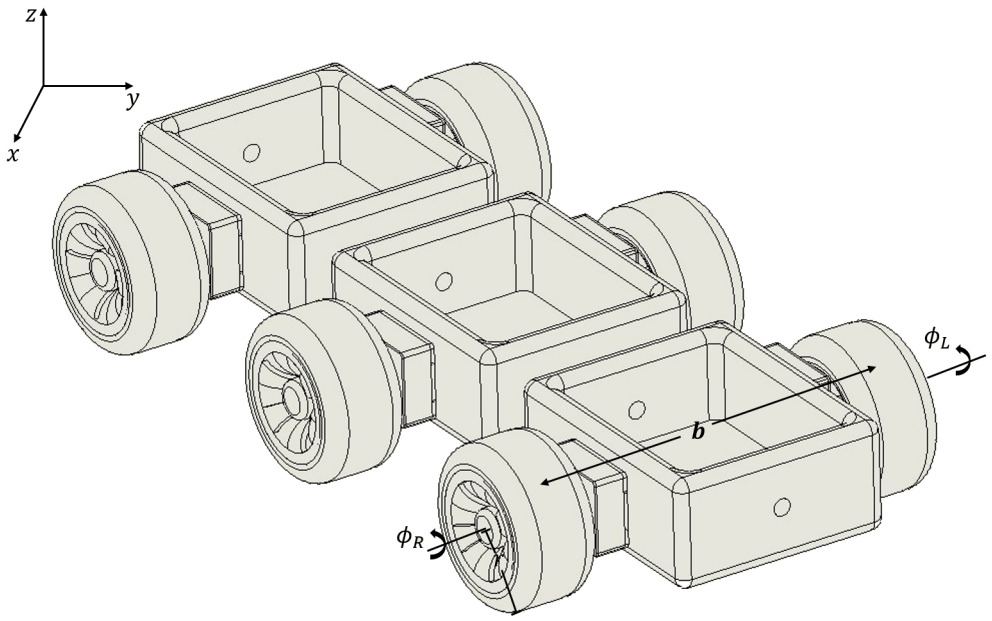

Figure 8: *Configuración de robot vehícular*

In the 2W2D configuration, both the pitch mechanism and the prismatic mechanism are disabled, leaving only the yaw mechanism enabled. Thus, according to Proposition 4, the following recoinfiguration conditions established:

$$\dot{\theta}_1 = -\left(\frac{4r_{s4}^2 r_0 r_5 n_2}{(r_{s4}+r_{a4})^2 r_1 r_6 n_3}\right)\dot{\phi}_0,\ \forall\ \dot{\phi}_0 = 0 \therefore \dot{\theta}_1 = 0,$$

$$\dot{d}_{T36} = L\left(\frac{16r_s^4}{(r_s+r_a)^4}\right)\dot{\phi}_{29},\ \forall\ \dot{\phi}_2 9 = 0 \therefore \dot{d}_{T36} = 0$$

and $\dot{\theta}_0$ is redefined as

$$\kappa_{R,L} = \left(\frac{r_{19} r_{22} n_{21}}{r_{20} r_{23} n_{22}}\right). \tag{112}$$

From this analysis, we derive the matrix-based model of direct kinematics,

$$\underbrace{\begin{pmatrix} v \\ \omega \end{pmatrix}}_{\dot{\mathbf{u}}} = \underbrace{\begin{pmatrix} \frac{r}{2} & \frac{r}{2} \\ \frac{2r}{b} & \frac{-2r}{b} \end{pmatrix}}_{\mathbf{K}} \underbrace{\begin{pmatrix} \kappa_R \dot{\phi}_{19R} \\ \kappa_L \dot{\phi}_{19L} \end{pmatrix}}_{\dot{\Theta}}, \tag{113}$$

Hence, the first-order derivative model of direct kinematics is:

$$\dot{\mathbf{u}} = \mathbf{K} \cdot \dot{\Theta} \tag{114}$$

Expressing it as a first-order linear differential equation, we can solve it using the method of separation of variables and derivatives with respect to dt and by integrating with respect to both differentials, the control law is established as

$$\Theta_{t+1} = \Theta_t + \mathbf{K}^{-1} \left(\mathbf{u}_{ref} - \mathbf{u}_t \right), \tag{115}$$

and

$$\mathbf{u}_{t+1} = \mathbf{u}_t + \mathbf{K} \left(\Theta_{t+1} - \Theta \right). \tag{116}$$

7.2 SCARA reconfiguration

The positional model of the SCARA configuration, which represents its spatial coordinates, is pivotal for understanding its positioning within the workspace and subsequently deducing its higher-order derivatives. These expressions serve as fundamental equations that characterize the relation-

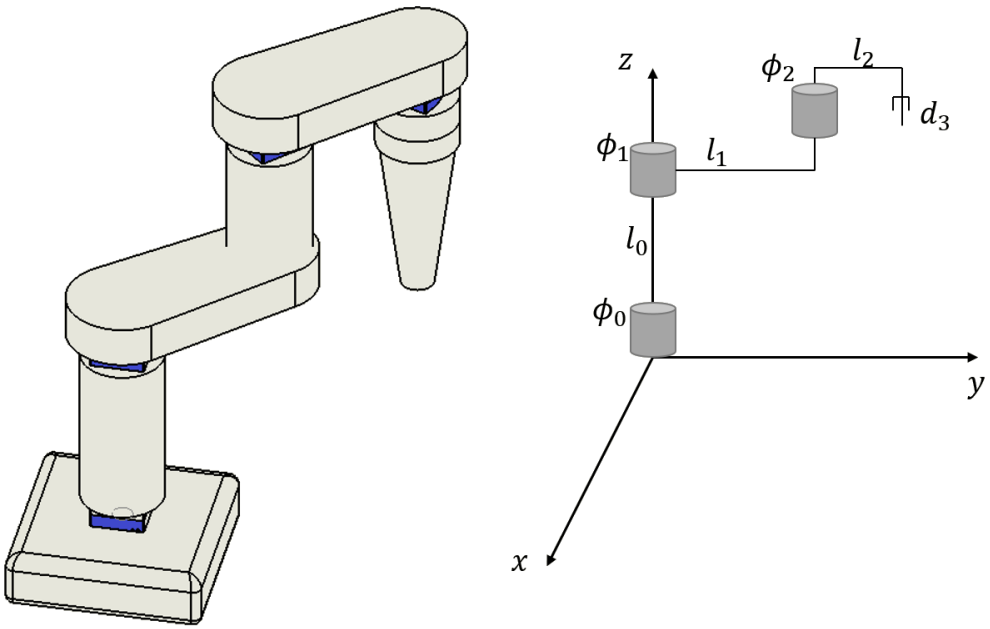

Figure 9: *Free body diagram of a SCARA platform using modular joints and links.*

ship between the SCARA robot's joint variables and its position in the Cartesian space. Through these analytical equations the robot's movements are controlled ensuring precise positioning.

$$x = l_1 \cos\left(\phi_0 + \phi_1\right) + l_2 \cos\left(\phi_0 + \phi_1 + \phi_2\right), \tag{117}$$

$$y = l_1 \sin\left(\phi_0 + \phi_1\right) + l_2 \sin\left(\phi_0 + \phi_1 + \phi_2\right), \tag{118}$$

$$z = d_3. \tag{119}$$

In previous Figure 9, we observe ϕ_0, ϕ_1, ϕ_2, and d_3, all of which are directly controlled by the intrinsic variables of the modular mechanism. In this specific SCARA configuration, both pitch and prismatic movements are disabled for $\phi_{0,1,2}$, while for d_3, pitch and yaw movements are disabled. Hence, we initially consider the intrinsic variables of the module for $\phi_{0,1,2}$ with the following reconfiguration conditions,

$$\dot{\theta}_1 = -\left(\frac{4r_{s4}^2 r_0 r_5 n_2}{(r_{s4}+r_{a4})^2 r_1 r_6 n_3}\right)\dot{\phi}_0,\ \forall\ \dot{\phi}_0 = 0 \therefore \dot{\theta}_1 = 0,$$

and

$$\dot{d}_{T36} = L\left(\frac{16r_s^4}{(r_s+r_a)^4}\right)\dot{\phi}_{29},\ \forall\ \dot{\phi}_2 9 = 0 \therefore \dot{d}_{T36} = 0.$$

And once again, $\dot{\theta}_0$ is redefined as

$$\kappa_{0,1,2} = \left(\frac{r_{19}r_{22}n_{21}}{r_{20}r_{23}n_{22}}\right), \tag{120}$$

while for $\dot{d}_3$, we consider the intrinsic variables as follows:

$$\dot{\theta}_0 = \left(\frac{r_{19}r_{22}n_{21}}{r_{20}r_{23}n_{22}}\right)\dot{\phi_{19}},\ \forall\ \dot{\phi}_{19} = 0 \therefore \dot{\theta}_0 = 0,$$

$$\dot{\theta}_1 = -\left(\frac{4r_{s4}^2 r_0 r_5 n_2}{(r_{s4}+r_{a4})^2 r_1 r_6 n_3}\right)\dot{\phi}_0,\ \forall\ \dot{\phi}_0 = 0 \therefore \dot{\theta}_1 = 0,$$

and

$$\dot{d}_3 = \dot{d}_{T36d3} = L\left(\frac{16r_s^4}{(r_s+r_a)^4}\right)\dot{\phi}_{29d3}.$$

In this way, the matrix model of direct kinematics is represented by:

$$\underbrace{\begin{pmatrix}\dot{x}\\ \dot{y}\\ \dot{z}\end{pmatrix}}_{\dot{\mathbf{u}}} = \underbrace{\begin{pmatrix}-l_1\sin(\kappa_0+\kappa_1)-l_2\sin(\kappa_0+\kappa_1+\kappa_2) & -l_1\sin(\kappa_0+\kappa_1)-l_2\sin(\kappa_0+\kappa_1+\kappa_2) & -l_2\sin(\kappa_0+\kappa_1+\kappa_2) & 0\\ l_1\cos(\kappa_0+\kappa_1)+l_2\cos(\kappa_0+\kappa_1+\kappa_2) & l_1\cos(\kappa_1+\kappa_2)+l_2\cos(\kappa_0+\kappa_1+\kappa_2) & l_2\cos(\kappa_0+\kappa_1+\kappa_2) & 0\\ 0 & 0 & 0 & 1\end{pmatrix}}_{\mathbf{K}} \underbrace{\begin{pmatrix}\dot{\kappa}_0\phi_{190}\\ \dot{\kappa}_1\phi_{191}\\ \dot{\kappa}_2\phi_{192}\\ \dot{d}_{T36d3}\phi_{293}\end{pmatrix}}_{\Theta} \tag{121}$$

Therefore, the direct kinematics model, expressed as first-order derivatives, is

$$\dot{\mathbf{u}} = \mathbf{K}\cdot\dot{\Theta} \tag{122}$$

This can be formulated as a first-order linear differential equation, which is solved using the method of separating variables and derivatives with respect to dt, and upon integrating with respect to both differentials, the control law is established as

$$\Theta_{t+1} = \Theta + \mathbf{K}^{-1}\left(\mathbf{u}_{ref} - \mathbf{u}_t\right), \tag{123}$$

and

$$\mathbf{u}_{t+1} = \mathbf{u}_t + \mathbf{K}\left(\Theta_{t+1} - \Theta\right). \tag{124}$$

7.3 Configuration of multi-link manipulator

In this section, we unveil a conceptual crafting approach along with a positional model tailored for a robotic multi-link configuration. Emphasizing the significance of crafting reconfigurability on manipulators, Figure 10 illustrates this model, highlighting the modular mechanism, alongside its free body diagram delineating spatial coordinates.

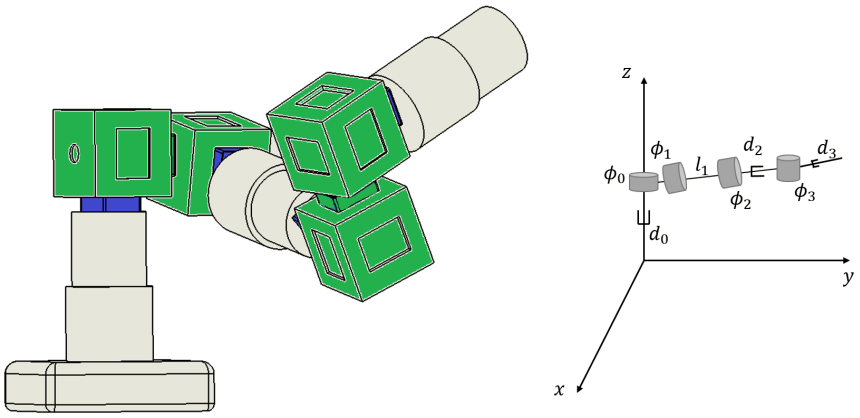

Figure 10: *M*ulti-link robot manipulator and free body diagram.

The following expressions represent the position model with respect to the coordinates of the workspace of the manipulator configuration:

$$x = (l_1 + d_2 + d_3 \cos\phi_3 \sin\phi_2)\cos\phi_1, \tag{125}$$

as well as

$$y = (l_1 + d_2 + d_3 \sin\phi_3)\sin\phi_1, \tag{126}$$

and

$$z = d_0 + (l_1 + d_2 + d_3 \cos\phi_2 \cos d_3)\sin\phi_1. \tag{127}$$

The coefficients corresponding to each intrinsic variable undergo redefinition. In this structural scenario, there are no configuration restrictions, necessitating that all degrees of freedom within each module remain enabled.

$$\kappa_{0,4,6} = \left(\frac{16r_s^4}{(r_s + r_a)^4}\right); \quad \kappa_{1,3} = \left(\frac{r_{19}r_{22}n_{21}}{r_{20}r_{23}n_{22}}\right); \quad \kappa_{2,5} = -\left(\frac{4r_{s4}^2 r_0 r_5 n_2}{(r_{s4} + r_{a4})^2 r_1 r_6 n_3}\right). \tag{128}$$

When substituting the intrinsic variables in the models of spherical coordinates, we have:

$$\dot{x} = \left(l_1 + \kappa_4\dot{\phi}_{294} + \kappa_6\dot{\phi}_{296}\cos\kappa_5\dot{\phi}_{05}\sin\kappa_3\dot{\phi}_{193}\right)\cos\kappa_2\dot{\phi}_{02} \tag{129}$$

$$\dot{y} = \left(l_1 + k_4\dot{\phi}_{294} + \kappa_6\dot{\phi}_{296}\sin\kappa_5\dot{\phi}_{05}\right)\sin\kappa_2\dot{\phi}_{02} \tag{130}$$

$$\dot{z} = \kappa_0\dot{\phi}_{290} + \left(l_1 + \kappa_4\dot{\phi}_{294} + \kappa_6\dot{\phi}_{296}\cos\kappa_3\dot{\phi}_{193}\cos\kappa_6\dot{\phi}_{296}\right)\sin\kappa_2\dot{\phi}_{02} \tag{131}$$

8 Discussion Results

The outcomes obtained in this study are crucially discussed, highlighting the significance of the module's application in assembling various robotic platforms. Through a meticulous examination of the configurations of the gear mechanisms and the subsequent mathematical derivations, the

relevance of the results becomes apparent. Visual representations in the form of graphs provide a clear illustration of the angular position of each gear within the pitch mechanism, as outlined by equations 15 to 20 in Definition 2, showcased in Figure 11. Notably, by enveloping the kinematic models of the gears within a sinusoidal function, a discernible reduction in the movement of gears $e_{4,5}$ and e_6 relative to gears e_{1-3} is observed, underscoring the practical implications of the findings for optimizing robotic mechanisms and enhancing their operational efficiency. Similarly, the

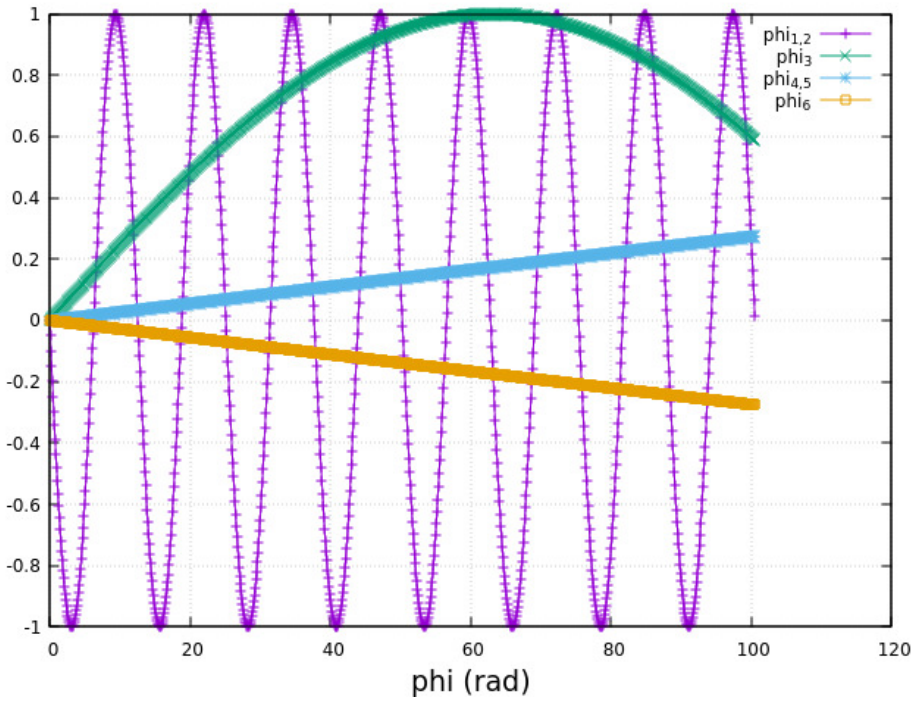

Figure 11: *Angular positions of the gears within the pitch mechanism.*

angular positions of the gears within the yaw mechanism, crucial for the module's functionality, as delineated by equations 22 to 26 in Definition 3, are vividly illustrated in Figure 12. This depiction is pivotal for understanding the operational dynamics of the robotic module. Notably, a significant reduction in speed is discerned among gears $e_{22,23,24}$ compared to gears $e_{20,21}$, underscoring the module's ability to control and modulate motion effectively.

In terms of the motion dynamics of the planetary gears constituting the prismatic mechanism, as defined in Definition 4 and derived from equations 30 and 32, the contents of this analysis hold significant relevance. The data series within this mechanism exhibit notable overlap, a phenomenon arising from the inherent parallelism of the mechanical connection between the two planetary gears, as vividly illustrated in Figure 13. Understanding this overlap is crucial as it underscores the intricate mechanical structure of the module and its implications for motion control and stability.

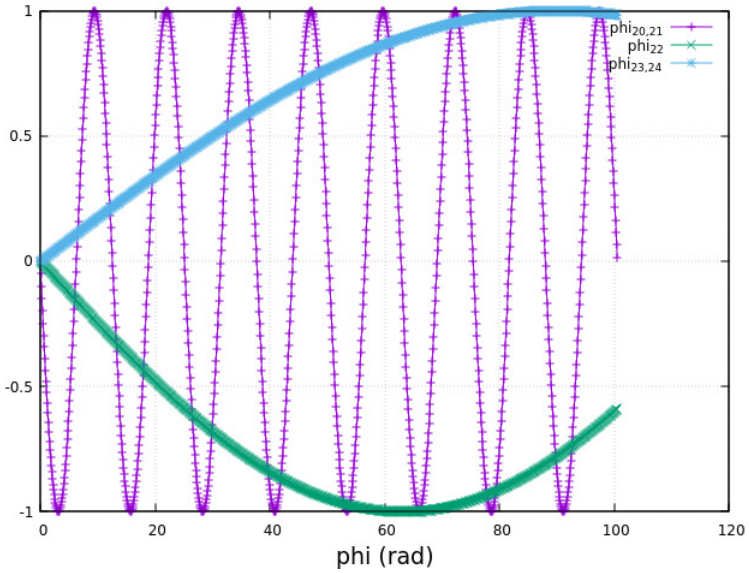

Figure 12: *Angular positions of the gears in the yaw mechanism.*

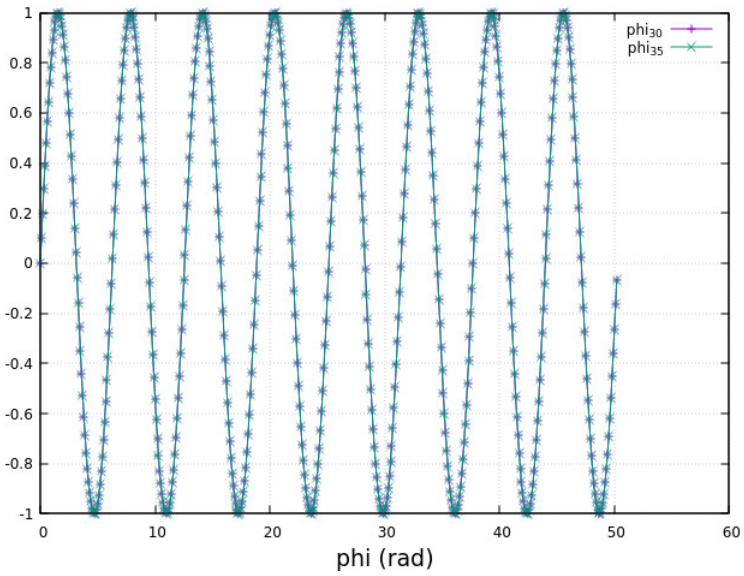

Figure 13: *Angular positions of the gears in the prismatic mechanism.*

Concerning the dynamic capability of the pitch mechanism as detailed in Definition 6, with specific emphasis on Theorem 1, torque values were systematically generated by conducting angular position sweeps and varying angular accelerations. This experimental procedure, illustrated in Figure 14, is crucial for evaluating the mechanism's ability to handle dynamic loads effectively, highlighting its operational robustness and performance reliability.

Similarly, the examination of the dynamic capabilities of the yaw mechanism, as defined in Definition 7 and elaborated in Theorem 1, involved mapping torque values across angular position sweeps and a range of angular accelerations, a critical analysis depicted in Figure 14.

Furthermore, an equivalent investigation was conducted to assess the dynamic potential of the prismatic mechanism, outlined in Definition 8. Utilizing Theorem 3, a thorough exploration of torque values was meticulously charted through angular position sweeps and various angular accelerations, an essential aspect of the discussion portrayed in Figure 14. These analyses are vital as they offer valuable insights into the mechanisms' ability to effectively handle dynamic loads, highlighting their operational robustness and performance reliability.

9 Conclusion

The primary goal of this research was to create a modular system enabling the assembly of diverse robotic platforms, flexible in configuration to enhance their functional capabilities. The design of multiple components was executed at the CAD level. This approach facilitated the generation of various module prototypes, streamlining modifications and expediting the physical system modeling process until achieving an optimal module with the desired functions. Regarding the design of the three mechanisms composing the module, coherence was found between the mechanical advantages of these mechanisms and the necessary parameters in the workspace.

Sensor models were incorporated to measure dynamic variables such as position, velocity, and acceleration, integrating them into the kinematic and dynamic equations of the three mechanisms. Although the study's primary focus was on the dynamic modeling of mechanisms, it was necessary to develop a physical model as a starting point for deducing kinematic, kinetic, and dynamic models. The models were validated in C++, chosen for its rapid control capability and high numerical precision. Overall, all numerical calculations were executed in short times.

Despite the widespread adoption of other controllers in modern control theory, this project opted to establish control models based on the physics of the modular mechanism. The advantage of this approach lies in the natural deduction of physical parameters, such as inertia, mass, and gravity, as opposed to requiring trial-and-error parameters adjustment.

The development of a modular system capable of assembling diverse robotic platforms offers future researchers and engineers the advantage of rapid prototyping and customization. This modularity can streamline the design and development process for a wide range of robotic applications, from industrial automation to mobile robotics. Moreover, by executing component designs at the CAD level and streamlining the prototyping process, future projects can benefit from reduced design iteration times. This efficiency allows for quicker exploration of design alternatives and optimization of functional capabilities. In addition, leveraging double planetary gear systems, as identified in the project, can provide future robotic platforms with increased stability and torque amplification. This advantage is particularly beneficial for applications requiring precise control and manipulation tasks, such as robotic arms or articulated mechanisms. The validation of kinematic, kinetic, and dynamic models in C++ provides an approach in predicting system behavior, facilitating the development of control algorithms and trajectory planning methods. The deduction of theorems describing the matrices of instantaneous torques for each mechanism offers a principled approach to control system design. Opting for control models based on the physics of the modular mechanism provides a distinct advantage in deducing physical parameters such as inertia, mass, and gravity.

The conclusions drawn from this project suggest several key trends shaping the technological and scientific development within the field of robotics. First, the ongoing evolution of modular robotics platforms is poised to persist, enabling the assembly of diverse robotic systems with enhanced flexibility and adaptability. This trend will likely drive future research towards refining modularity to accommodate a wider array of applications. Second, there is a noticeable shift towards integrating advanced control and sensing techniques into robotic systems, signifying a move towards more autonomous and capable robots. This trajectory will likely lead to the exploration of new sensor technologies and control algorithms to further enhance robot performance and autonomy. Third, the streamlining of design iterations, as demonstrated in this project, is anticipated to become increasingly prevalent, driving the development of more efficient design tools and methodologies for rapid prototyping and optimization. Additionally, the pursuit of stability and precision in robotic design, particularly through mechanisms like double planetary gear systems, is expected to persist, fostering innovations in motion control and stability augmentation. Lastly, the trend towards application-driven research is anticipated to continue, with a focus on

developing robotic solutions tailored to specific real-world needs across various domains, from industrial automation to healthcare. Overall, these trends underscore the ongoing advancement of robotics technology towards increasingly sophisticated and impactful applications.

References

[1] Rosyid A., Stefanini C., El-Khasawneh B., *A Reconfigurable Parallel Robot for On-Structure Machining of Large Structures*. *Robotics*. 2022; 11(5):110.

[2] Mahmood F., Hashemi SM., Alighanbari H., *Free Vibration Analysis of a Reconfigurable Modular Morphing Wing. Aerospace*. 2022; 9(10):532. https://doi.org/10.3390/aerospace9100532

[3] M. Vega, E.A. Martínez-García, R. Torres-Cordoba, *Unstructured terrain adaptive navigation of self-reconfigurable quadruped robot*, *IFAC-papers online*, 48(19) 2015, pp. 183-188, Elsevier.

[4] Kulandaidaasan J., Mohan R.E., Martínez-García E.A., Tan-Phuc Le., *Synthesizing reconfigurable foot traces using a Klann mechanism. Robotica.* Cambridge University Press, Vol.33, Mar 2015.

[5] Sheba J.K., Mohan R.E., Martínez-García E.A., Tan-Phuc L., *Trajectory Generation and Stability Analysis for Reconfigurable Klann Mechanism based Walking Robot. Robotics.* 5(3),13; pp. 1-20, mdpi, 2016

[6] Guan Y., Zhuang Z., Zhang C., Tang Z., Dai J.S., *Design and Motion Planning of a Metamorphic Flipping Robot.Actuators.* 2022; 11, 344.

[7] Moosavian A., Xi F., Hashemi S.M., *Design and Motion Control of Fully Variable Morphing Wings.Journal of Aircraft.* 2013; 50(4), 11891201.

[8] Fei F., Leng Y., Xian S., Dong W., Yin K., Zhang G., *Design of an Origami Crawling Robot with Reconfigurable Sliding Feet. Appl. Sci.* 2022, 12, 2520.

[9] Sahin E., Girgin S., Bayindir L., Turguta E., *Swarm robotics, swarm intelligence: Introduction and applications.* In Christian Blum, Daniel Merkle (eds) *Swar Intelligence Introduction and Applications.* Berlin, Germany: Springer, 2008, pp. 87-100

[10] Wei H., Chen Y., Tan J., Wang T.,*Sambot: A Self-Assembly Modular Robot System. IEEE/ASME Transactions on Mechatronics.* (2011)16(4), 745-757.

[11] Li H., Wang H., Cui L., Li J., Wei Q., Xia J., *Design and Experiments of a Compact Self-Assembling Mobile Modular Robot with Joint Actuation and Onboard Visual-Based Perception. Appl. Sci.* 2022, 12, 3050.

[12] Peck R.H., Timmis J., Tyrrell A.M., *Self-Assembly and Self-Repair during Motion with Modular Robots. Electronics.* 2022, 11, 1595.

[13] Saeed R.A., Tomasi G., Carabin G., Vidoni R., Von Ellenrieder K.D., *Conceptualization and Implementation of a Reconfigurable Unmanned Ground Vehicle for Emulated Agricultural Tasks.Machines.* 2022, 10, 817.

[14] Taira T., Kamata N., Yamasaki N., *Design and implementation of reconfigurable modular humanoid robot architecture. 2005 IEEE/RSJ Intl. Conf. on Intelligent Robots and Systems* Edmonton, AB, Canada, 2005, pp. 3566-3571.

[15] Ao W., Zhang L., Zhang H., Li Z., Huang G., *Structure Design and Event-Triggered Control of a Modular Omnidirectional Mobile Chassis of Life Support Robotics. Fractal Fract.* 2023, 7, 121. https://doi.org/10.3390/fractalfract7020121

[16] Yi L., Le A.V., Hoong J.C.C., Hayat A.A., Ramalingam B., Mohan R.E., Leong K., Elangovan K., Tran M., Bui M.V., Duc P.V., *Multi-Objective Instantaneous Center of Rotation Optimization Using Sensors Feedback for Navigation in Self-Reconfigurable Pavement Sweeping Robot. Mathematics.* 2022, 10, 3169. https://doi.org/10.3390/math10173169

[17] Semwal A., Lee M.M.J., Sanchez D., Teo S.L., Wang B., Mohan R.E.,*Object-of-Interest Perception in a Reconfigurable Rolling-Crawling Robot. Sensors.* 2022, 22, 5214. https://doi.org/10.3390/s22145214

[18] Qi Z., Wang H., Huang Z., Zhang L., *Kinematics of a quadruped/biped reconfigurable walking robot with parallel leg mechanisms. 2009 ASME/IFToMM International Conference on Reconfigurable Mechanisms and Robots.* London, 2009, pp. 558-564.

[19] Merlet J.P., *Determination of the optimal geometry of modular parallel robots. 2003 IEEE International Conference on Robotics and Automation.* (Cat. No.03CH37422), Taipei, Taiwan, 2003, pp. 1197-1202 vol.1, doi: 10.1109/ROBOT.2003.1241755.

[20] Liu H., Wang H., Li S., He L., *Research on the topology description and modeling method for reconfigurable modular robots. 2009 ASME/IFToMM International Conference on Reconfigurable Mechanisms and Robots.* London, UK, 2009, pp. 129-135.

[21] Marschall M., Gregor M., Ďurica L., Vavrík V., Bielik T., Grznár P., Mozol Š., *Defining the Number of Mobile Robotic Systems Needed for Reconfiguration of Modular Manufacturing Systems via Simulation. Machines.* 2022, 10, 316. https://doi.org/10.3390/machines10050316

[22] Ahmed R.M., Ananiev A.V., Kalaykov I.G., *Safe robot with reconfigurable compliance/stiffness actuation. 2009 ASME/IFToMM International Conference on Reconfigurable Mechanisms and Robots.* London, UK, 2009, pp. 603-608

[23] Dasi S., Malladhi N., Tigadi A., Majji S., Patnala T.T., Reddy V.P., *Adaptable Reconfigurable and Power-Efficient Robots for Health Monitoring. 2022 Second International Conference on Advances in Electrical, Computing, Communication and Sustainable Technologies (ICAECT).* Bhilai, India, 2022, pp. 1-4, doi: 10.1109/ICAECT54875.2022.9808048.

[24] Pisla D., Plitea N., Vidrean A., Prodan B., Gherman B., Lese D., *Kinematics and design of two variants of a reconfigurable parallel robot. 2009 ASME/IFToMM International Conference on Reconfigurable Mechanisms and Robots.* London, UK, 2009, pp. 624-631.

[25] Sun T., Song Y., Li Y., Zhang J., *Stiffness estimation for the 4-DOF hybrid module of a novel reconfigurable robot. 2009 ASME/IFToMM International Conference on Reconfigurable Mechanisms and Robots.* London, UK, 2009, pp. 565-571.

[26] Charles River Editors *The Antikythera Mechanism: The history and mystery of the ancient world's most famous astronomical device.*

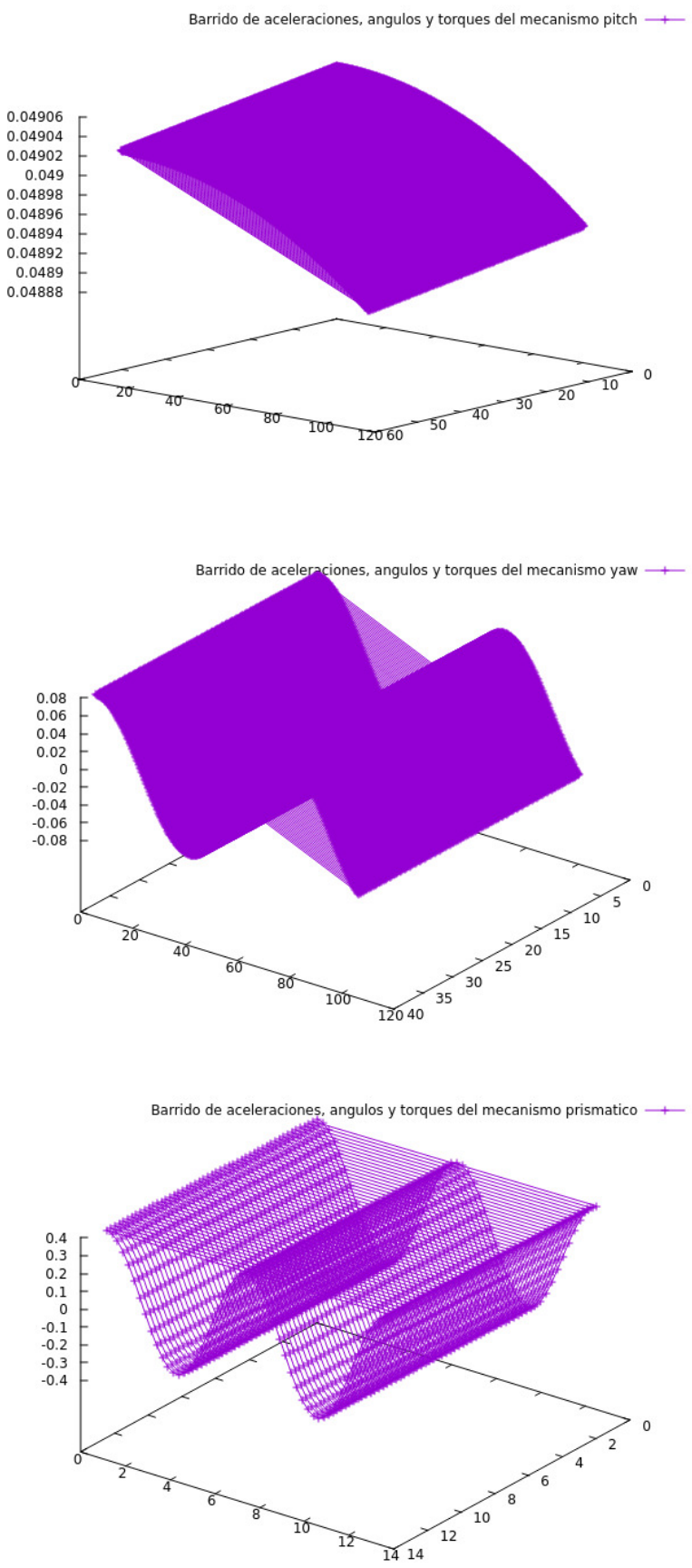

Figure 14: Sweeping of accelerations, angles y torques for the pitch, yaw and linear mechanisms.